THE GIANTS OF THE PHYLUM BRACHIOPODA: A MATTER OF DIET?

LUCIA ANGIOLINI[1]*, GAIA CRIPPA[1], KAREM AZMY[2], GIANCARLO CAPITANI[3], GIORGIA CONFALONIERI[4], GIOVANNA DELLA PORTA[1], ERIKA GRIESSHABER[5], DAVID A.T. HARPER[6], MELANIE J. LENG[7,8], LEAH NOLAN[9], MARCO ORLANDI[3], RENATO POSENATO[10], WOLFGANG W. SCHMAHL[5], VANESSA J. BANKS[8], MICHAEL H. STEPHENSON[8]

[1]Dipartimento di Scienze della Terra "A. Desio", Via Mangiagalli 34, 20133, Milano, Italy; e-mails: Lucia.angiolini@unimi.it, gaia.crippa@unimi.it, giovanna.dellaporta@unimi.it

[2]Department of Earth Sciences, Memorial University of Newfoundland, St. John's, NL A1B 3X5, Canada; e-mail: kazmy@mun.ca

[3]Dipartimento di Scienze dell'Ambiente e del Territorio e di Scienze della Terra, Piazza della Scienza 4, 20126 Milano, Italy; e-mail: giancarlo.capitani@unimib.it, marco.orlandi@unimib.it

[4]Dipartimento di Scienze della Terra, Università degli Studi di Torino, Torino, Italy; e-mail: giorgia.confalonieri@unito.it

[5]Department für Geo- und Umweltwissenschaften, Ludwig-Maximilians Universität München, Munich, Germany; e-mails: e.griesshaber@lrz.uni-muenchen.de, Wolfgang.W.Schmahl@lrz.uni-muenchen.de

[6]Department of Earth Sciences, Durham University, Durham DH1 3LE, UK; e-mail: david.harper@durham.ac.uk

[7]NERC Isotope Geosciences Facilities, British Geological Survey, Keyworth, Nottingham NG12 5GG, UK; e-mail: mjl@bgs.ac.uk

[8]British Geological Survey, Keyworth, Nottingham, NG12 5GG, UK; e-mails: mjl@bgs.ac.uk, mhste@bgs.ac.uk, vbanks@bgs.ac.uk

[9]Department of Geology, University of Leicester, University Road, Leicester, LE1 7RH, UK

[10]Dipartimento di Fisica e Scienze della Terra, Via Saragat, 1, 44121 Ferrara, Italy; e-mail: renato.posenato@unife.it

Abstract: The species of the brachiopod *Gigantoproductus* are giants within the Palaeozoic sedentary benthos. This presents a dilemma as living brachiopods have low-energy lifestyles. Although brachiopod metabolic rates were probably higher during the Palaeozoic than today, the massive size reached by species of *Gigantoproductus* is nevertheless unusual. By examining the diet of *Gigantoproductus* species from the Visean (Mississippian, Carboniferous) of Derbyshire (UK), we seek to understand the

mechanisms that enabled those low-metabolism brachiopod species to become giants. Were they suspension feeders, similar to all other brachiopods or did endosymbiosis provide a lifestyle that allowed them to have higher metabolic rates and become giants? We suggest that the answer to this conundrum may be solved by the identification of the biogeochemical signatures of symbionts, through combined analyses of the carbon- and nitrogen-isotopic compositions of the occluded organic matrix within their calcite shells. The shells are formed of remarkably long, and a few hundreds of micrometres wide, substructured columnar units deemed to be mostly pristine based on multiple analyses [petrography, cathodoluminescence (CL), Scanning Electron Microscopy (SEM), Electron Backscatter Diffraction (EBSD), Transmission Electron Microscopy (TEM)]; they contain occluded organic fractions detected by TEM, Nuclear Magnetic Resonance (NMR), and Gas Chromatography Mass Spectrometry (GC-MS) analyses. We conclude that the gigantic size reached by the species of *Gigantoproductus* is probably the result of a mixotroph lifestyle, by which they could rely on the energy and nutrients derived both from photosymbiotic microbes and from filtered particulate food.

Key words: *Gigantoproductus,* gigantism, brachiopods, diet, endosymbiosis, Carboniferous

The species of *Gigantoproductus* are notable giants within the Brachiopoda, attaining sizes of more than an order of magnitude higher than all other members of this marine phylum of lophotrochozoans. They reach over 30 cm in width and over 1 cm in shell thickness (e.g., Muir-Wood & Cooper 1960; Angiolini *et al.* 2012; Qiao & Shen 2015; Vermeij 2016). Living brachiopods have a low-energy lifestyle (low metabolism, low growth, feeding and reproduction rates) (e.g., Curry *et al.* 1989; Peck 1996; Vermeij 2016), and so the size of *Gigantoproductus* is puzzling, though the reason for this has never been investigated in detail nor satisfactorily explained. Brachiopod metabolic rates were probably higher and more variable during the Palaeozoic (Payne *et al.* 2014; Vermeij 2016) and brachiopods had a trend towards larger size (Novack-Gottshall & Lanier 2008; Zhang *et al*. 2015). The size reached by species of *Gigantoproductus* is, nonetheless, still dramatically larger compared with the average size of other Palaeozoic brachiopods. The size increase during the Palaeozoic has been attributed to increases in available oxygen, primary productivity, and predation pressure (e.g., Zhang *et al.* 2015); although other recent studies (e.g., Vermeij 2016) emphasized that the gigantism of fossil and

recent plants and animals remains poorly understood. Gigantism has been interpreted as an evolutionary strategy for protection against predators, because the cost of killing and consuming prey is higher than the benefit (Palmer 1999; Vermeij 2012). The early growth stages of giant prey, when the individual is more vulnerable, are characterized by rapid growth (Vermeij 2012). However, competitive interactions, more than predation, may have been the main reason for gigantism (Vermeij 2016).

One of the key features of gigantism is a high metabolic rate (Vermeij 2016), apparent also in the case of marine ectotherms such as normal suspension feeders, photosymbiotic and chemosymbiotic animals. In the latter, the larger the size, the higher the activity levels and metabolic rates, and symbiotic associations are known to have frequently led to gigantism (Vermeij 2016). Through removal of CO_2, algal symbiosis also promotes calcification leading to skeletal gigantism (Cowen 1983; Key *et al.* 2005). This has been demonstrated in Recent and fossil foraminifera, corals and bivalves (e.g., Vogel 1975; Lee *et al.* 1979; Cowen 1988). Similarly, the large size of the Permian lyttonioid and richthofenioid brachiopods is thought to have been related to their tropical distributions and possible association with zooxanthellae algae (Cowen 1970); an attractive hypothesis established on the basis of their large size and comparison with the giant bivalve *Tridacna* and its symbionts. Other brachiopods from deep time have been hypothesized to have reached a very large size through methano- or thiotrophic diets, such as the Lower Cretaceous rhynchonellid *Peregrinella* (e.g., Campbell & Bottjer 1995; Posenato & Morsilli 1999; Kiel *et al.* 2014).

Gigantism is also reported in species recording the ‘gentle giant syndrome’**.** These species live under conditions with poor resources – such as those in the polar regions and the deep sea - and are characterized by low metabolic rates, slow-growth, minimal maintenance costs, and low juvenile mortality (e.g., Antarctic marine animals and island tortoises; Arnaud 1974; Rosa & Seibel 2010; Vermeij 2016).

Here, we investigate and seek to understand the mechanisms that enabled ectothermic, low-metabolism and physiologically unbuffered brachiopod species with a primitive lophophore to become giants. We examine their feeding strategy and whether they were normal suspension feeders as typical for all other brachiopods, or influenced by an endosymbiotic lifestyle that possibly enabled them to have higher metabolic rates and become giants.

One of the best ways to evaluate these causes is to look for the biogeochemical signatures that identify symbioses (e.g., Levin & Michener 2002; O'Donnell *et al.* 2003;

Mae *et al.* 2007; Dreier *et al.* 2012, 2014), such as the carbon and nitrogen isotope composition ($\delta^{13}C_{org}$, $\delta^{15}N_{org}$) of the primary organic fraction occluded in the shell, after the evaluation of its degree of preservation. To discriminate between a suspension-feeding lifestyle versus a symbiotic lifestyle, we compared different species of *Gigantoproductus* occurring together in different palaeoenvironmental settings (Nolan *et al.* 2017).

MATERIAL AND METHODS

Fifty specimens of *Gigantoproductus elongatus* (Pattison, 1981), *Gigantoproductus inflatus* (Sarytcheva, 1928) and *Gigantoproductus okensis* (Sarytcheva, 1928), from the Derbyshire Platform, Visean (Mississippian, Carboniferous) Monsal Dale Limestone and Eyam Limestone formations of Ible (specimens id "IB"), Wensley Dale (specimens id "WI"), Once-a-Week Quarry (specimen id "OAW") and Ricklow Quarry (specimens id "RCK") in Derbyshire, UK (Fig. 1, Table 1A-B), were measured to quantify their size [for details on their provenance and depositional environment see Angiolini *et al.* (2012) and Nolan *et al.* (2017)]. Sixteen specimens from the Once-a-Week and Ricklow quarries were used for petrographic and cathodoluminescence analyses, and ten specimens were selected for ultrastructural (SEM, TEM, EBSD), oxygen and carbon isotope analyses of calcite, and carbon and nitrogen isotope analyses of occluded organic material. Nuclear magnetic resonance and GC-MS analyses were performed on the shell organic matrix of specimen RCK16. The specimens are permanently curated in the Palaeontological Museum of the Department of Earth Sciences 'A. Desio', University of Milan, Italy and registered with a prefix MPUM (11800-11815).

In addition, 69 specimens of species belonging to genera other than *Gigantoproductus* , co-occurring with *Gigantoproductus* in the same formations at Ible, Wensley Dale, Once-a-Week Quarry and Ricklow Quarry were also measured for size (Table 1B).

Petrographic and CL analyses

Sixteen brachiopod shells of *G. okensis*, *G. inflatus* and *G. elongatus* from the Eyam Limestone Formation at Once-a-Week Quarry (OAW3, OAW8, OAW50, OAW203, OAW205, OAW209, OAW212) and Ricklow Quarry (RCK11, RCK16, RCK33, RCK35, RCK36, RCK41, RCK100, RCK221, RCK300) were embedded in resin, cut longitudinally and thin sectioned. Petrographic analysis was performed with a polarized light optical microscope. Cathodoluminescence (CL) was performed using a cold stage cathode

luminoscope (CITL Cambridge Image Technology Limited, Cambridge, UK, model MK 5-2) operating at 10-14 kV accelerating voltage with a beam current of 200-300 μA at the Department of Earth Sciences 'A. Desio', University of Milan, Italy. The CL is a screening technique widely used for the preliminary assessment of preservation of brachiopod shells (e.g., Angiolini *et al.* 2009; Garbelli *et al.* 2012, 2014).

SEM, TEM and EBSD analyses

To further assess shell preservation and the reliability of the isotope data, several screening techniques were applied to ten selected specimens (OAW3, OAW203, OAW212, RCK16, RCK33, RCK35, RCK36, RCK41, RCK221, and RCK300). Their ultrastructure was examined by Scanning Electron Microscope (SEM), Transmission Electron Microscope (TEM), and Electron Backscatter Diffraction (EBSD). The sectioned specimens were etched with 5% HCl for 20 s before coating with gold to examine the preservation of their shell fabric under SEM following the methodology described in Angiolini *et al.* (2008, 2009).

TEM mounts were prepared from epoxy embedded samples and doubly-polished petrographic thin sections (30 μm thick) were prepared. Electron transparency was achieved by ion milling 3 mm wide discs cut out from the petrographic thin sections using a Gatan PIPS (Department of Earth Sciences 'A. Desio', University of Milan, Italy). The TEM mounts were then carbon coated to avoid electrostatic charging during observation. TEM observations were performed with a Jeol JEM 2010 operating at 200 kV and equipped with an Oxford Link energy dispersive spectrometer (EDS) and with an Olympus Tengra 2.3k x 2.3k x 14 bit slow-scan CCD camera (Department of Physics, Earth and Environment, University of Siena, Italy).

For Electron Backscatter Diffraction (EBSD) analyses, 5 x 5 mm thick pieces were excised from the shell and embedded in epoxy resin. The surface of the embedded samples was subjected to several sequential mechanical grinding and polishing steps down to a grain size of 1 μm. The final step was etch-polishing with colloidal alumina (particle size ~ 0.06 μm) in a vibratory polisher. For EBSD analysis, the samples were coated with 4-6 nm of carbon. EBSD measurements were carried out on Hitachi SU5000 field emission SEM, equipped with a Nordlys-II EBSD detector. The SEM was operated at 20 kV and measurements were indexed with the CHANNEL 5 HKL software. Information obtained from EBSD measurements is presented as band contrast images, and as colour-coded crystal orientation maps with corresponding pole figures, the latter displaying in one set of pole

figures the data points and, in a second set, calculated calcite c- and a*-axes data density distributions. The EBSD band contrast is the signal strength of the EBSD-Kikuchi diffraction pattern and is displayed as a grey-scale component in EBSD maps. The strength of the EBSD signal is high when a crystal is detected (bright in the map), while it is weak or absent when a polymer such as an organic fraction is scanned (dark/black in the map).

The brachiopod specimens OAW3, OAW203, OAW212, RCK16, RCK33, RCK35, RCK36, RCK41, RCK221, and RCK300 were sampled for geochemical and stable isotope analyses using a hand-held microdrill at low speed. Several grams (10-20 g) were taken from the middle part of the very thick columnar shell layer of the ventral valve using a diamond drill bit carefully avoiding to sample secondary fractures filled by burial diagenesis calcite and marginal shell portions affected by silicification. When sufficient powder was obtained, it was split into two parts, one for carbon and oxygen isotope analysis on shell calcite (10 specimens), and the other one for nitrogen and carbon isotope measurements on organic fraction isolated from the shell (six specimens). RCK16 was also sampled for Nuclear Magnetic Resonance (NMR) and Gas Chromatography Mass Spectrometry (GC-MS) analyses on shell organic matrix.

O and C stable isotopes from shell calcite and O isotopes of silica

The stable isotope ratios of shell calcite were measured on shells OAW3, OAW203, OAW212, RCK16, RCK33, RCK35, RCK36, RCK41, RCK221 and RCK300 at the British Geological Survey, Nottingham, UK. Approximately 50-100 µg of calcite was used, and analysed for C and O isotope ratios using an Isoprime dual inlet mass spectrometer plus Multiprep device. Samples were loaded into glass vials and sealed with septa. The automated system evacuates vials and delivers anhydrous phosphoric acid to the carbonate at 90ºC. The evolved CO_2 is cryogenically cleaned and passed to the mass spectrometer. Isotope values ($\delta^{13}C$, $\delta^{18}O$) are reported as per mil (‰) deviations of the isotopic ratios ($^{13}C/^{12}C$, $^{18}O/^{16}O$) calculated to the VPDB scale using a within-run laboratory standard calibrated against NBS-19. The Craig correction is also applied to account for ^{17}O (Craig 1957). Analytical reproducibility for the standard calcite (KCM) and sample material was < 0.1‰ for $\delta^{13}C$ and $\delta^{18}O$ [(both 1 standard deviation (SD)].

Classical fluorination with the step wise approach is employed at the British Geological Survey for the oxygen isotope analysis of silica. The method involves a three-stage process. Stage one involves 'outgassing' to remove surficial and loosely bound water; stage two involves a prefluorination step involving a stoichiometric deficiency of the reagent chlorine trifluoride (ClF_3) at low temperature; and the third stage is a full reaction

at high temperature for an extended period with an excess of reagent. The oxygen liberated is then converted to CO_2 by exposure to graphite. Oxygen yields were monitored by comparison with the calculated theoretical yield for SiO_2. Isotope values ($\delta^{18}O$) are reported as per mil (‰) deviations of the isotopic ratio ($^{18}O/^{16}O$) calculated to the VSMOW scale using a within-run laboratory standard calibrated against NBS-28. Analytical reproducibility of the standard silica (BFC) and sample material was < 0.3‰ for $\delta^{18}O$ (1SD).

C and N isotopes from shell organic fraction

Carbon and nitrogen isotope ratios of the organic fraction were measured on shells OAW212, RCK16, RCK33, RCK36, RCK41 and RCK300 at Memorial University of Newfoundland, St. John's, Canada. Several grams of powder were obtained from six brachiopod specimens and weighed into 150 mL glass beakers. A total of 100 mL of 6M distilled HCl diluted to 20% was added gradually in 10 mL increments over a period of several days. The samples were stirred after each addition of HCl until there was no visible reaction. After the carbonate reaction was complete, the samples were transferred to centrifuge tubes to remove the acid and retain the organics and silicates. This residue was rinsed into 15 mL Teflon jars using deionised water and left to evaporate. Approximately 2 mL HF and 2 mL 6.2N HCl was added to the sample, covered and left on a hot plate for 4-5 days; heating was not vigorous (around 50°C, to prevent alteration of the organic matrix). The cover was removed, rinsed and the sample left to evaporate. Two mL of 6.2N HCl were added and evaporated twice. The sample was rinsed into microcentrifuge tubes using deionised water and left to evaporate.

Organic carbon ($\delta^{13}C_{org}$) and nitrogen ($\delta^{15}N_{org}$) isotope ratios were measured on isolated kerogen after repeated treatment with pure concentrated hydrochloric acid, using a Carlo Erba Elemental Analyzer coupled to a Thermo Fisher DELTA V plus isotope ratio mass spectrometer in a stream of helium, where the gas was ionized and measured for isotope ratios. The results were normalized to the standards IAEA-CH-6 ($\delta^{13}C$ = –10.4 ‰ VPDB), NBS-18 ($\delta^{13}C$ = –5.0 ‰ VPDB), USGS-24 ($\delta^{13}C$ = –16.0 ‰ VPDB), IAEA-N-1 ($\delta^{15}N$= +0.4 ‰ air), and IAEA-N-2 ($\delta^{15}N$= +20.3 ‰ air). Based on repeated measurements of $\delta^{13}C$ and $\delta^{15}N$ standards (organic), uncertainty was ~ 0.2 ‰.

GC-MS and ^{1}H-NMR analyses on shell organic fraction

The pulverized RCK16 samples (around 10 g) were dried in an oven 2 h at 90°C and then were dewaxed by washing three times with diethyl ether (100 mL) under magnetic stirring and sonication. The powders were recovered by paper filtration. The dewaxed fossil samples were hydrolyzed with 200 mL of 2 M HCl under vigorous magnetic stirring and at the end of the reaction, the pH of the suspensions was adjusted at around 7 by the addition of 5 M NaOH dropwise. The suspensions were then lyophilized overnight in order to obtain a white powder.

^{1}H-NMR analysis. The white powder was extracted with 200 mL of a solution 20:80 v/v of chloroform:methanol under magnetic stirring and sonication. The organic phase was recovered by filtration and then the solvent was distilled under vacuum. The residue was suspended in $CDCl_3$ and submitted to ^{1}H-NMR analysis by Bruker 600 MHz.

GC-MS analysis. Two methods were followed: A) the white powder was suspended in 150 mL of dry methanol and then 0.5 mL of 98% H_2SO_4 were added in order to promote the methylation of carboxylic acids. The suspension was refluxed 5 h and then, after cooling, it was diluted with 200 mL of distilled water and neutralized with $NaHCO_3$ until pH 9. The suspension was then extracted by diethyl ether (3 times with 100 mL). The organic phase was treated with anhydrous $NaSO_4$ and then dried in rotavapor. The residue was dissolved in CH_2Cl_2 and then submitted to GC-MS analysis. B) the white powder (1 g) was suspended in 1 mL of acetonitrile/water and then it was derivatized by the addition of 500 µL of isobutanol, 300 µL of pyridine and 250 µL of isobutylchloroformiate. After 30 minutes, 1 mL of chloroform was added and the vial was shaken. After phase separation, the organic layer (2 µL) was submitted to GC-MS analysis.

RESULTS

Size of the species of Gigantoproductus *from the Visean of Derbyshire*

To quantify the size of *Gigantoproductus* species in comparison with the average size of co-occurring Palaeozoic taxa, we measured the width and length of 50 specimens of *G. elongatus*, *G. inflatus* and *G. okensis* and of 69 specimens of species of brachiopod genera other than *Gigantoproductus* belonging to four different orders (Productida, Rhynchonellida, Spiriferida, Terebratulida) from the Visean Monsal Dale Limestone and Eyam Limestone formations from the Ible, Wensley Dale, Once-a-Week and Ricklow quarries (Table 1A-B). All the size measurements are in mm and shell areas in millimetres squared (mm^2). Following the method of Zhang *et al.* (2015), we calculated the log-transformed shell area, where the shell area is the product of measured width and length

(in mm). The average log-transformed shell area of the species of *Gigantoproductus* is 4.0, and the maximum recorded value is 4.3. By comparison, the log-transformed shell area of the other non-gigantoproductid brachiopod taxa associated with the species of *Gigantoproductus* is lower, around 2.4. In other words, the average shell area of species of *Gigantoproductus* is 11393 mm^2, whereas that of species of associated genera is 679 mm^2.

Shell preservation

Based on a combination of petrographic (Fig. 2; Angiolini *et al*. 2019, fig. S1), CL (Fig. 3; Angiolini *et al*. 2019, fig. S2), SEM (Fig. 4; Angiolini *et al*. 2019, fig. S4), TEM (Figs 5-6), and EBSD examinations (Fig. 7), ten specimens of *G. okensis*, *G. inflatus* and *G. elongatus* were found to be the best preserved (Table 2) and were thus selected for stable isotope analyses. The ventral valve of most of the specimens has a pseudopunctate laminar secondary layer, occasionally preserved, and a well-preserved thick columnar tertiary layer (Fig. 2A-B).

Petrographic investigation shows that the analysed shells are locally altered by authigenic silica replacement (Fig. 2C-F). This occurs as a brownish, fibrous chalcedony (mostly length-slow quartzine followed by length-fast chalcedonite) and anhedral to subhedral microquartz forming concentrically laminated spherulites with undulose extinction (from 0.5 mm to several millimetres in size elongated parallel to shell boundary), and euhedral megaquartz crystals with hexagonal basal section, sometimes with undulose extinction (from 0.2 mm up to several millimetres in size), which embed calcite crystals and growth lines of the brachiopod shells. The observed types of silicification are described in previous studies (Folk & Pittman 1971; Maliva & Siever 1988; Daley & Boyd 1996) and resemble those classified by Schmitt & Boyd (1981) as pattern II and V for the silicification of Permian bivalves and brachiopods.

Chalcedony spherulites may be the only type of silica replacement present or they can be adjacent to hexagonal quartz crystal clusters or overgrown by euhedral quartz (Fig. 2C), as also observed through SEM analysis (Fig. 4). In the ventral valves, chalcedony spherulites occur along the outer margin of the columnar layer aligned parallel to it, or at or close to the boundary between the columnar tertiary and laminar secondary layer when present, especially at the boundaries between individual columnar crystals. Less frequently, chalcedony spherulites and megaquartz are observed along the internal margin of the columnar layer and very rarely in the middle portion of the ventral valve. The dorsal

valves appear more affected by silicification, especially on the laminar layer and on the inner and outer margins of the columnar layer (Fig. 2D), but also across the entire valve thickness, in particular towards the umbonal region and anterior margin (Angiolini *et al*. 2019, fig. S1). Chalcedony spherulites are affected by stylolites and cut by fractures filled by burial calcite cement (Fig. 2E-F) suggesting that they formed relatively early during burial diagenesis before mechanical compaction, pressure solution and brittle fracturing occurred. Euhedral megaquartz crystals followed the formation of chalcedony spherulites, overgrowing them but they also formed independently, in particular on the laminar secondary layer.

X Ray Powder Diffraction (XRPD) analyses of powders extracted from the gigantoproductids confirm the presence of quartz with a variable crystallinity index (from 5.43 to 7.26 out of a maximum of 10) as calculated following Marinoni & Broekmans (2013), which revised that of Murata & Norman (1976) (Angiolini *et al*. 2019, fig. S3). This method has the advantage of being rather simple allowing crystallinity index determination by inspecting the height of the quartz (212) reflection. The low crystallinity of some analysed samples might be related to the chalcedony spherulites mixed with the quartz crystals because the two phases could not be separated during the extraction of the sample powders. $\delta^{18}O$ in the quartz phases of four gigantoproductid shells provide an average $\delta^{18}O$ of +29.5 ‰ (V-SMOW) indicative of quartz precipitation at low temperature (up to 45-50°C calculated based on the equations of Clayton *et al.* 1972 and Murata *et al.* 1977). This suggests that silica replacement of the gigantoproductid outer shell occurred during early diagenetic phases rather than during deep burial, supporting the petrographic observation that chalcedony spherulites formed before compaction (stylolite) and fracture formation. Orme (1973) evaluated the variety of chert and sphaerulitic chalcedony to quartz observed in the Visean Derbyshire limestones suggesting that replacement of the host limestone appeared to have occurred prior to its complete consolidation. According to Hollis (1998), silicification of the Derbyshire platform limestones occurred in various phases during burial diagenesis at temperatures of 60-100°C and burial depths of 1-2 km during the Serpukhovian-Bashkirian (Namurian).

The analysed shells displayed variable responses to cathodoluminescence (Fig. 3; Angiolini *et al*. 2019, fig. S2) ranging from non-luminescent to partially- or fully-luminescent, indicative of variable degrees of diagenetic alteration (e.g., calcite recrystallization and replacement during burial diagenesis, silicification, calcite and dolomite precipitation in fractures). The ventral valve appeared better preserved than the

dorsal valve (Fig. 3A-B; Angiolini *et al*. 2019, fig. S2A-D) and in particular, the columnar layer of the ventral valve was non-luminescent, except locally along a few secondary fractures, boundaries between columnar crystals and the outer and inner margins of the tertiary layer where it is silicified (Table 2). In the ventral valve, the secondary laminar layer, when present, and the outer and inner margins of the tertiary columnar layer appear bright luminescent with evidence of calcite recrystallization, associated with silicification (Fig. 3A-D), in particular towards the umbonal region and anterior margin. Growth lines show a weak luminescence, but this may be a primary feature (Angiolini *et al.* 2008, 2009). Fractures (from a few microns up to 1 mm wide) might occur filled either by bright luminescent calcite or dull luminescent calcite followed by dolomite euhedral rhombs (Fig. 3E-F). The dorsal valves often exhibit bright luminescence with evidence of calcite crystal replacement, silicification and fracture-filling bright luminescent sparite (Fig. 3A-B; Angiolini *et al*. 2019, fig. S2D-F).

Thus, the central portion of the columnar tertiary layer in the middle part of the ventral valve, away from fractures cutting the shell, appears to be the best preserved part of the investigated gigantoproductid valves. These parts were therefore sampled for stable isotope analyses (Table 2).

The Derbyshire platform limestones were affected by diagenesis during burial with precipitation of several calcite phases and dolomite within fractures (e.g., Hollis 1998). Burial history curves constructed by Hollis (1998) and Breislin (2018) suggest a maximum burial temperature for the Brigantian on the Derbyshire Platform of 110-120°C (assuming a geothermal gradient of 30°C/km) and a maximum depth of burial of 3-4 km during the Serpukhovian to Moscovian post-rift thermal subsidence before the Variscan Orogeny basin inversion. Burial diagenesis and the flow of burial brines were controlled by Caledonian-Variscan faults and fractures (Hollis & Walkden 1996; Hollis 1998; Hollis & Walkden 2002), but our sample localities are not affected by these faults and fractures. SEM analysis confirms that shell fabric is pristine (Fig. 4). The microstructure is a three-layered rhynchonelliformean architecture (Williams & Cusack 2007), with thin cross-bladed laminar secondary and a thick columnar tertiary layers, but the primary layer is absent due to dissolution. There is no sign of calcite crystals with a rhombohedral morphology in the columnar layer, which argues against alteration (Casella *et al.* 2018a). The columnar microstructure (Fig. 4 C-D) is very similar to that of Recent brachiopods (see figs 1-2 in Ye *et al.* 2018a; and plate 4A-C in Ye *et al.* 2018b) suggesting that the preservation of the tertiary layer of the selected specimens is very good, except for the outer margins around

chalcedony spherulites and megaquartz. In any case, these outer regions were avoided when sampling for geochemistry. Altered specimens that were not selected for study have lost the columnar fabric and are often highly silicified over the entire shell thickness (see Angiolini *et al*. 2019, fig. S4).

TEM analyses of shell RCK16 (*G. okensis*) (Figs 5-6) show that the columnar layer is formed by nanoscopic, biocomposite mesocrystal calcite (*sensu* Casella *et al.* 2018a), that is built up by grains approximately co-oriented and with the c-axis lying on the plane of observation (the longitudinal section of the brachiopod shell; Fig. 5A), as observed in Recent taxa (Ye *et al.* 2018a).

EBSD analyses show that the original shell microstructures are well preserved, with the shells still showing the presence of large columnar units with crystallites being highly co-oriented (Figs 7A-C). The MUD values of the three samples (OAW203, RCK16, RCK 221) are 71, 48 and 41, respectively. According to Casella *et al.* (2018a, b), MUD values of well-preserved brachiopods range between 40 and 80 (exceptionally being over 100); moderately to fairly well-preserved brachiopod shells have MUD values between 20 and 40, and overprinted brachiopod shells have MUD values lower than 20. This suggests the *Gigantoproductus* shells used for geochemical analyses are indeed well preserved. Occasionally the shell margins are overprinted (Fig. 7B), but this is readily seen, as randomly oriented calcite crystallites completely destroy the original microstructure, and have low MUD values of around 14. These materials were not used for analyses.

Finally, oxygen and carbon isotope data from the shell calcite are within the range of values (respectively –4.7‰ to –3.4‰ and +0.8‰ to +2.6‰; Table 2) previously reported for pristine shells of Visean species of *Gigantoproductus* (Popp *et al.* 1986; Armendáriz *et al.* 2008; Angiolini *et al.* 2012). The mean $\delta^{18}O$ values of the Carboniferous (mean±1σ) in Veizer *et al*. (1999) vary from –5±3 ‰ (Mississippian) to –2.5±1‰ (Pennsylvanian) and our results are within this range. Similar values were also reported for the Visean by Bruckschen *et al.* (1999) with $\delta^{18}O$ between –7‰ and –2‰ and $\delta^{13}C$ between +1‰ and +6 ‰, and by Grossman *et al.* (2008) with $\delta^{18}O$ between –5‰ and –2‰ and $\delta^{13}C$ between +1‰ and +4‰.

The Sr, Mn and Fe contents of the brachiopod shells are given in Angiolini *et al*. (2019, fig. S5) and the data fit within the range of trace elements values reported for modern brachiopods and for well-preserved Palaeozoic brachiopods (Angiolini *et al.* 2009 and references therein).

Organic fraction occluded in the calcite of the columnar layer of the brachiopod shell

TEM analyses of the columnar shell layer RCK16 (*G. okensis*) show that it consists of nanoscopic, biocomposite mesocrystalline calcite. The calcite grains contain a large number of dispersed, intragranular, oval inclusions, with dimensions ranging from less than 10 nm to ~100 nm in diameter. From the contrast in the bright field images, the largest inclusions are polyphasic and contain: 1) a void, possibly filled by a gas; 2) an amorphous material (which is either a fluid, a glass, a gel, or unrecognizable) with a darker tone due to a mass-thickness contrast; and 3) sometimes a solid, possibly a crystalline precipitate, with a euhedral habit and characterized by a very dark tone due to high diffraction contrast (Fig. 5B-C). The largest inclusions are often connected by dislocations (Fig. 6A), which are especially visible close to the <1-1 0> zone, and may form trails along dislocation lines (Fig. 6B). Finally, we found a different type of inclusion, a few nanometres in size, with a dark contrast, forming trails between calcite grain borders (Fig. 6C) similar to those observed by Schmahl *et al.* (2012) in Recent brachiopod shells.

These organic inclusions within the shell were analysed in the preserved columnar layer of one of the specimens (RCK16) by nuclear magnetic resonance and GC-MS. The ^{1}H-NMR analysis shows clusters at 1.90, 1.70, 1.45 ppm typical of amino acid aliphatic chains such as alanine, leucine or isoleucine (Fig. 8A). A cluster observed at 2.90-2.80 ppm may be explained as being a lateral chain of aspartate/asparagine (Fig. 8B).

In order to confirm these preliminary results, GC-MS analysis was performed using two different kinds of derivatization. First, a Fisher derivatization was performed to transform the carboxylic function of amino acids in a methyl ester derivatives. More than 15 different acids with aliphatic chains were detected, not necessary amino acids, but all with relatively high molecular weight; so that the low molecular weight amino acids such as glycine or alanine were impossible to detect. In order to overcome this masking problem, the sample was derivatized with isobutylchloroformiate before running the GC-MS to derive the ammines and eventually the amide function. The chromatogram of GC-MS analysis shows more than 50 different peaks corresponding to organic compounds and at least 10 with the typical fragmentation of aliphatic amino acids. At this level it is not possible to attribute the type of amino acid by mass fragmentation in GC-MS, but according to the results of ^{1}H-NMR and GC-MS, it is possible to ascertain that there are several aliphatic amino acids in RCK16, particularly alanine, leucine and serine.

Isotope geochemistry of shell organic fraction

$\delta^{13}C_{org}$ and $\delta^{15}N_{org}$ were measured in organic fractions isolated from the nanoscopic biocomposite mesocrystalline calcite of the preserved part of the columnar layer of six specimens of two species of *Gigantoproductus* (*G. inflatus* and *G. okensis;* Table 3). They all reach a gigantic size and have the same lifestyle, but in two different shallow-water settings: high-energy crinoidal shoals in inner ramp settings at Once-a-Week Quarry and within the shelter provided by relict mud mounds in middle ramp settings at Ricklow Quarry (Nolan *et al.* 2017).

The $\delta^{13}C_{org}$ values are typically low and range from –25.9 to –29.0 ‰, while $\delta^{15}N_{org}$ varies between –2.0 to +4.1 ‰ at both localities (Table 3) and are apparently unrelated to a taxon-specific effect or any palaeoecological constraints. In particular, $\delta^{13}C_{org}$ is rather uniform, with only one specimen of *G. okensis* from Ricklow Quarry having a slightly higher value. Unlike $\delta^{13}C_{org}$ values, more variation occurs within the $\delta^{15}N_{org}$ data. Three specimens of *G. inflatus* and *G. okensis* from Ricklow Quarry have positive values, whereas a specimen each of *G. inflatus* from Ricklow and Once-a-Week Quarry have slightly negative values. There is no relationship between each species, their palaeoenvironmental setting, and the isotope data. The correlation between $\delta^{15}N$ and $\delta^{13}C$ is poor (R^2=0.24), and the data are scattered around the regression line and not tightly clustered which does not support the absolute p value (significance level). This is consistent with the low R2 values of $\delta^{15}N_{org}$ vs TOC (0.17) and $\delta^{13}C_{org}$ vs TOC (0.002). These correlations do not support significant or consistent changes in the $\delta^{15}N$ and $\delta^{13}C$ values with their corresponding TOC values (Azmy *et al*. 2015).This argues against covarying post-depositional diagenetic alteration.

Finally, measurements of $\delta^{15}N$ and $\delta^{13}C$ in low concentration samples are more accurate than low abundance C and N concentration measurements. We assume that the C/N ratio data are inaccurate because of the low %N. The C/N is high which could be due to preferential loss of N. There are no studies known by the authors on how N loss affects $\delta^{15}N_{org}$ in marine fauna, but studies of C loss in plants show that the $\delta^{13}C_{org}$ change is small (Schleser *et al.* 1999; Smith *et al.* 2017).

DISCUSSION

Are Gigantoproductus *species true giants?*

Our results show that the size reached by *Gigantoproductus* species is significantly larger than the average size of all other Palaeozoic brachiopods. The mean body size of all

Carboniferous brachiopods measured by Zhang *et al.* (2015) as log-transformed shell area (shell areas measured in mm^2) is around 2.6, comparable with the value of 2.5 obtained for non-gigantoproductid brachiopods from the Visean of Derbyshire. The same parameter measured for *Gigantoproductus* species is up to 4.3, their average shell area being nearly the double of that of the other Visean taxa. This is consistent with the survey of giants throughout the Phanerozoic by Vermeij (2016) who considered *Gigantoproductus* as one of the largest sedentary bottom-dwellers of the Palaeozoic.

Growth rates in *Gigantoproductus* were high, especially at the juvenile stages, as shown by growth line spacing and by the growth curve published by Angiolini *et al.* (2012, fig. 6). Based on sclerochronology and on spiral deviation analysis, Angiolini *et al.* (2012) showed that the lifespan of a large *G. okensis* was 20 years, in agreement with the survival rates of extant brachiopods, and in no way comparable to the Recent longest–living bivalve *Arctica islandica* with a lifespan of at least 500 years (e.g., Butler *et al.* 2013). So extreme longevity cannot be the cause of *Gigantoproductus* gigantism. There are Recent bivalves that reach a large size through rapid growth [as species of *Crassostrea*, (e.g. Chávez-Villalba *et al.* 2005)], but they are efficient suspension-feeder capable of qualitative particle selection (Decottignies *et al*., 2007).

The largest Recent brachiopod species is the terebratulide *Magellania venosa* (Dixon, 1789) which has an average length between 30-45 mm, and a maximum length of 70 mm (McCammon 1973; Baumgartner *et al.* 2014). This translates into an average log-transformed shell area of 3.2 and a maximum log-transformed shell area of 3.6, which are lower than the values calculated for our *Gigantoproductus* species. Furthermore, *Magellania venosa* is usually very thin-shelled, its shell thickness being 1-2 mm (e.g., Cohen *et al*., 2011; Ye *et al*. 2019), even though an unpublished specimen from Huinay Station is 5 mm-thick in section (Elizabeth Harper, pers. comm.). In comparison, *Gigantoproductus* is a very thick-shelled brachiopod (c. 10 mm), generating substantial amounts of calcium carbonate. In contrast with its giant size, the lophophore of *Gigantoproductus* is quite simple, as shown by the brachial ridges in the dorsal valve (Fig. 9; Muir-Wood & Cooper 1960; Angiolini *et al.* 2012), accompanied by a pair of conical pits (brachial cones) deeply impressed in the shell substance of the ventral valve (Fig. 9; Muir-Wood & Cooper 1960; Angiolini *et al.* 2012). These features suggest the presence of a schizolophe lophophore similar to that reconstructed by Brunton (1982, fig. 13) for the Visean productid *Levitusia*, where the direction of current inflow and outflow has been recently interpreted as consisting of lateral inhalant currents and a median exhalant

current (Shiino & Suzuki 2011). Brunton himself (1982, p. 161-162) was surprised by the contrast between the low efficiency of the small and simple reconstructed lophophore and the size and thickness of the shell of *Levitusia,* so that he suggested that nutrition could have been sustained by absorption of nutrients by the epithelium.

On the other hand, *Levitusia* (with a log-transformed shell area of about 3.3) is smaller than *Gigantoproductus*, with a thinner shell.

A comparison with the lophophore type of the largest Recent brachiopod *M. venosa* emphasizes even more the disparity between the size of the species of *Gigantoproductus* and their simple type of lophophore. *M. venosa* has a plectolophe lophophore, which is the most complex of the coiled feeding organs (MacKinnon & Lee 2006) and allows the animal to acquire and assimilate more food resources than other invertebrates (McCammon 1973, p. 271). The plectolophe type is developed at the adult stage after transition through different stages which are much simpler [trocholophe – schizolophe - zygolophe (Emig 1992)]; the schizolophe in particular (i.e. the *Gigantoproductus* type of lophophore) is typical of the larval and juvenile stages of *M. venosa*. This is also explicitly demonstrated in the diagrams of LaBarbera (1986, figs 1-2, p. 317) which scale the total lophophore area to the ash-free dry masses (AFDM) of the soft tissues of two terebratulide species with plectolophe lophophore: they have a schizolophe lophophore at small body masses (0.05 to 0.4 mg AFDM), and a plectolophe lophophore at body masses greater than 0.5 mg up to 900 mg.

Alternative explanations are clearly required to explain how the large size of *Gigantoproductus* species was achieved with a simple schizolophe lophophore. In addition, most *Gigantoproductus* species lack a median sulcus, which, as shown by Emig (1992) and Shiino & Kuwazuru (2011), has a very important role in increasing the efficiency of the lophophore by creating water currents flowing over the tentacles and enhancing food acquisition.

An hypothesis is that of a symbiotic lifestyle which may be tested through the analysis of the $\delta^{13}C_{org}$ and $\delta^{15}N_{org}$ of the preserved organic matrix of the shell (cf. O'Donnell *et al.* 2003; Mae *et al.* 2007; Dreier *et al.* 2012, 2014; Dreier & Hoppert 2014).

Is the shell-occluded organic fraction preserved?

Recent rhynchonelliformean brachiopods have a shell composed of calcite containing a minor organic fraction (less than 1% of the dry powder weight) that is involved in calcification and becomes occluded in the shell microstructure when formed (e.g. Immel *et*

al. 2015). TEM investigation during the current study has proved the occurrence of numerous nano-sized oval inclusions containing an amorphous material (fluid, gel or glass), a void (possibly filled by a gas) and sometimes a solid. It is worth noting that such oval inclusions do not occur in non-biogenic calcite prepared with ion milling techniques, and they cannot be related to calcite decomposition by electron beam damage, as they were present in the first observations. In addition, calcite decomposition in air commences at T > 600 °C (Rodriguez-Navarro *et al.* 2009), a temperature too high to be reached during ion milling. According to Park *et al.* (2007), the local temperature in a thin sample (200 nm) during ion-milling under typical conditions (6 KeV, beam incidence 10°, comparable to those employed here) depends on many factors, but especially on sample conductivity. The highest temperature value recorded after testing several materials is 330 °C for silica glass, therefore much lower than that required to initiate calcite decomposition. Moreover, calcite decomposition would result in the formation of CaO nanorods (Rodriguez-Navarro *et al.* 2009) in crystallographic relationship with the calcite single crystals, which we did not observe.

Skeletal carbonates, unlike non-biogenic carbonates, contain organics and comparatively large amounts (up to 3% weight) of water (Gaffey 1988; Casella *et al.* 2018a, b) which form an intrinsic part of the carbonate skeleton incorporated during growth. Organic material (as biopolymer membranes and network of fibrils) and water are intimately associated and are disseminated throughout skeletons in minute inter- and intra-crystalline cavities. The ovoidal inclusions we detected by TEM may represent evidence of these organic materials and water. These inclusions may have been trapped when solid or precipitated from the original fluid after its entrapment.

Microstructures very similar to those we observe have been reported by Ye *et al.* (2018a) from the tertiary layer of the Recent brachiopod *Liothyrella neozelanica.* They have also been reported in the secondary layer of both *L. neozelanic*a and *L. uva* by Goetz *et al.* (2011), who described “small somatoid (cigar-like) areas of lower density” in the primary layer of the Recent brachiopod *Gryphus vitreus.* Kelm *et al.* (2012) described similar inclusions in the spines of *Holopneustes porissisimus*.

Lécuyer & O’Neil (1994), in a study of stable isotopes in fluid inclusions within biogenic calcite, concluded that trapped fluids are the remnants of metabolic fluids and could provide information about metabolic activity recorded in well-preserved fossils. The key question is whether the inclusions are pristine or altered by diagenesis or any post-diagenetic events.

The samples selected for this study show fabrics consistent with primary growth mechanisms, free of signs of recrystallization, and show a microstructure very similar to those of modern brachiopods for which their optimal preservation state has been assessed (i.e., Goetz *et al.* 2011; Ye *et al.* 2018a, b). Almost certainly, intense deformation would breach fluid inclusions and cause exchanges with external fluids (Goldstein 1986). In the selected samples we used here, however, calcite grains are free of microstructures typical of deformation, such as deformation twins, undulose extinction, and healed fractures. On the other hand, since fluid entrapment occurred at ambient temperatures, some degree of natural heating during diagenesis may be expected. Heating causes internal overpressure that may be released by decrepitation, a leakage in the fluid inclusion content that can reequilibrate with the ambient pore fluid (Goldstein 2001). We explain the dislocations detected in some of our samples this way. However, whereas some degree of thermal reequilibration cannot be ruled out, thermal reequilibration did not necessarily affect every fluid inclusion in the mineral phase. In fact, not all the fluid inclusions are connected with dislocations, and it is generally observed that minute inclusions, such as those observed here, are more resistant to thermal reequilibration - a physical effect related to the very small size of the inclusions (Goldstein 2001). Moreover, whereas overpressure can cause fluid content to leak out of the inclusion, the reverse, i.e. the refill of the inclusion with foreign material through dislocations, is improbable. Therefore, if organic molecules were entrapped during crystal growth, it is likely that at least some of them could be preserved in the inclusions. Finally, the TEM investigation in the current study has proved the occurrence of nanometre-sized dark inclusions similar to those observed by Schmahl *et al.* (2012) and Casella *et al*. (2018a) in modern brachiopods and attributed to “intercrystalline organics”. Thus, at least some of the numerous inclusions revealed by TEM analyses are likely to be the remnants of occluded organic biopolymers within the columnar tertiary layer of calcite in the *Gigantoproductus* species shell.

The occurrence of organic matrix in the nanoscopic, biocomposite mesocrystal calcite of the columnar layer is also proven by NMR and GC-MS analyses, which show the presence of alanine, leucine/isoleucine, serine, and asparagine that occur in Recent rhynchonelliformean brachiopods (Immel *et al.* 2015). According to Cusack & Williams (2007), serine and asparagine occur in high concentrations also in the shells of *Novocrania*.

Although it is uncommon, the preservation of organic components inside fossil biominerals has been already documented by earlier studies (e.g., Cuif 1972; Sorauf 1999; O’Donnel

et al. 2003; Muscatine *et al*. 2005; Vandenbroucke & Largeau 2007 and references therein; Frankowiak *et al.* 2013; Yamazaki *et al.* 2013; Tornabene *et al.* 2017). Simple and robust amino acids (aspartic acid/asparagine, serine and glycine) have been extracted from Carboniferous cranioid and linguloid brachiopods, possibly preserved by interaction with the carbonate and apatitic matrices (Cusack & Williams 2007).

What diet enabled these species to become giants?

The biosignature associated with symbioses was investigated through the measurement of $\delta^{13}C_{org}$ and $\delta^{15}N_{org}$in the organic matrix extracted from the columnar tertiary layer calcite of *Gigantoproductus* species shells. These proxies are considered more robust for the detection of ancient symbioses than the $\delta^{13}C$ and $\delta^{18}O$ of the shell calcite. MacLeod & Hoppe (1992) interpreted enriched calcite $\delta^{13}C$ values from bivalve inoceramid shells as an indicator of a chemosymbiotic life-style. However, Grossman in Grossman *et al.* (1993) argued against this interpretation, as modern chemosymbiont-harbouring bivalves are depleted in ^{13}C relative to equilibrium. In their reply, MacLeod & Hoppe in Grossman *et al.* (1993) emphasized that "both enriched and depleted calcite ^{13}C values are found in the shells of chemosynthetic bivalves" and that more data from Recent shells are needed to discriminate between symbiotic and non-symbiotic life-styles based on shell carbonate stable isotopes. Stanley & Swart (1995) observed the wide range in the $\delta^{13}C$ and $\delta^{18}O$ values of modern scleractinian corals and considerable overlap between symbiotic and non-symbiotic species; however, skeletal samples from non-symbiotic corals always show a strong positive correlation between $\delta^{13}C$ and $\delta^{18}O$, which is not recorded in symbiotic corals. This was confirmed more recently by Rollion-Bard *et al*. (2003), who analysed $\delta^{13}C$ and $\delta^{18}O$ of recent azooxanthellate and zooxanthellate corals.

While the $\delta^{13}C$ and $\delta^{18}O$ of shell calcite from our *Gigantoproductus* species are within the range of values previously reported for Visean brachiopods (Veizer *et al*., 1999), there is no strong positive correlation between $\delta^{13}C$ and $\delta^{18}O$ (Table 2).

Jakubowicz *et al.* (2015) suggested that the isotopic signatures of Palaeozoic corals cannot be interpreted based on data from modern Scleractinia and so the absence of $\delta^{13}C$-$\delta^{18}O$ co-variance in Palaeozoic cnidarians cannot be interpreted as indicative of a photosymbiotic lifestyle. Others have also shown that the $\delta^{13}C$-$\delta^{18}O$ coral skeleton proxy can be used only in very few cases, because of the impact of diagenesis (Tornabene *et al.* 2017). It is beginning to be recognized that the $\delta^{15}N$ (and $\delta^{13}C$) of occluded organic material is much more robust and applicable, as the skeleton-bound organic matrix

remains preserved and protected from diagenesis by the skeletal structure itself (Tornabene *et al.* 2017).

It has been reported that soft tissues of filter-feeding bivalves in normal salinity ocean waters have a $\delta^{13}C_{org}$ ranging from –24 ‰ to –17 ‰ VPDB (Rau & Hedges 1979; Fry 1988; Kwak & Zedler 1997). Generally speaking, each increase in trophic level corresponds to a 1‰ soft tissue $\delta^{13}C_{org}$ enrichment relative to dietary carbon (e.g., O'Donnel *et al.* 2003). In contrast, soft tissues of chemosymbiotic organisms show a large $\delta^{13}C_{org}$ range from –70‰ to –15‰ (Nelson & Fisher 1995; Van Dover 2000; Mizota & Yamanaka 2003; Mae *et al.* 2007). In particular, chemosymbiotic bivalves show $\delta^{13}C_{org}$ values ranging from –35‰ to –27‰ (Childress & Fisher 1992; Robinson & Cavanaugh 1995; Cavanaugh *et al.* 2006).

The $\delta^{15}N_{org}$ values depend on the sources of the original nitrogen, but generally increase by 3.4‰ per trophic level (Minagawa & Wada 1984; Peirera *et al*. 2010). In marine primary consumers, the $\delta^{15}N_{org}$ values are between +8.4‰ and +9.5‰ and around +16.2‰ in tertiary consumers (Minagawa & Wada 1984). Marine filter-feeding bivalves have a range of $\delta^{15}N_{org}$ values from +6 to +14‰ (Minagawa & Wada 1984; Lorrain *et al.* 2002; Jennings & Warr 2003; O'Donnel *et al.* 2003). The soft tissues of chemosymbiotic animals have a wider $\delta^{15}N_{org}$ range, from –20‰ to +7‰, but the values are negative in most cases (Nelson & Fisher 1995; Van Dover 2000; Mizota & Yamanaka 2003; Mae *et al.* 2007).

In a recent study, Dreier *et al.* (2014) suggested that bulk organic shell matrices in Recent phototrophic and thiotrophic bivalves have lower $\delta^{13}C_{org}$ values (ranging from −31.0 ‰ to −25.5 ‰) than those of filter-feeding non-symbiotic bivalves where the latter have $\delta^{13}C_{org}$ values from −22.0 ‰ to −17.8 ‰. Comparable $\delta^{15}N_{org}$ values are −2.2‰to +0.1‰ for thiotrophic bivalves, +2.6‰ to +2.9‰ for phototrophic bivalves and +3.1‰ to +4.3‰ for filter-feeders. Correlation of the $\delta^{13}C_{org}$ and $\delta^{15}N_{org}$ values (Dreier *et al.* 2014, fig. 1) suggests that the chemosymbiotic lifestyle is characterized by low $\delta^{13}C_{org}$/low $\delta^{15}N_{org}$, the non-symbiotic lifestyle by high $\delta^{13}C_{org}$/high $\delta^{15}N_{org}$ and the phototrophic lifestyle by low $\delta^{13}C_{org}$/intermediate $\delta^{15}N_{org}$. This defines a fingerprint for distinguishing symbiotic from non-symbiotic lifestyles in living invertebrates. Muscatine *et al.* (2005), however, observed a highly significant difference in $\delta^{15}N_{org}$ between the coral skeletal organic matrix of Recent symbiotic and non-symbiotic corals, but not in $\delta^{13}C_{org}$; consequently, they considered $\delta^{15}N_{org}$ as a potential proxy for photosymbiosis. In particular, they found that $\delta^{15}N_{org}$ of the skeletal organic matrix of symbiotic corals is about 8‰ lower with respect to non-symbiotic corals. Tornabene *et al.* (2017) demonstrated the nitrogen isotopic ratio offset between

zooxanthellate- and azooxanthellate-corals and emphasized the robustness of the organic matrix $\delta^{15}N$ proxy for photosymbiosis.

According to Kirkendale & Paulay (2017), photosymbiotic metazoans do not rely entirely on symbiont-derived nutrition. In fact, some bivalves depend both on symbiont-fixed carbon and nitrogen together with filter feeding (e.g. Duplessis *et al.* 2004; Rossi *et al.* 2013 and references therein), so that their soft tissues record variable isotopic compositions ($\delta^{13}C_{org}$= –62‰ to –26‰; $\delta^{15}N_{org}$= –16‰ to +5‰; Pile & Young 1999; Dattagupta *et al.* 2004; McKiness *et al*. 2005; Mae *et al*. 2007). However, they apparently subsist more on symbiont-derived metabolites than on filter-feeding (e.g., Duperron *et al.* 2007; Dreier *et al.* 2014). Species of the same genus may show variation of ~ 5‰ in $\delta^{13}C_{org}$ and 1‰ in $\delta^{15}N_{org}$ (Dreier *et al.* 2014) depending on the proportion between the two nutrient sources (symbiosis vs. filter feeding). Rossi *et al.* (2013) reported variations of ~ 1‰ in $\delta^{13}C_{org}$ and 3‰ in $\delta^{15}N_{org}$ for individuals of a population of the mixotroph bivalve *Loripes lacteus* having different sizes and living in different positions of eelgrass meadows. A recent study on *Tridacna maxima* (Dreier *et al.* 2014) suggested that the proportion between the two lifestyles (symbiosis vs. filter feeding) may also change during ontogeny. Some studies of Triassic, Miocene and Pleistocene fossil shells (e.g. O'Donnell *et al.* 2003; Muscatine *et al*. 2005; Mae *et al.* 2007; Dreier *et al.* 2012; Tornabene *et al*. 2017) indicated that, under certain circumstances, it is possible to detect ancient symbioses using shell organic matrix carbon and nitrogen isotope signatures. Muscatine *et al*. (2005) were able to use this proxy on Upper Triassic corals from Turkey, confirming that *Pachythecalis major* (with a skeletal organic matrix $\delta^{15}N_{org}$ of 4.65‰) was most likely photosymbiotic, as already suggested by Stanley & Swart (1995). Tornabene *et al.* (2017) demonstrated a ~7‰ nitrogen isotopic ratio offset between zooxanthellate- and azooxanthellate-corals also in Triassic and Miocene fossil Scleractinia with different levels of diagenetic alteration. We have thus used these proxies to detect if *Gigantoproductus* species may have hosted symbionts.

One of the important achievements of the work of Mae *et al.* (2007) is the measurement of the differences between the isotopic values of the shell organic matrix (conchioline) and the soft tissues; the latter have lower $\delta^{13}C_{org}$ (about –3‰) and higher $\delta^{15}N_{org}$ (variable, but on average +1 ‰), which is consistent with the results of a later study by Dreier *et al.* (2012). As based on mollusc data, soft tissues have different isotopic values from shell organic matrix, to aid our discussion, we consider a simplified model of $\Delta^{13}C_{org}$ and $\Delta^{15}N_{org}$ between shell organic material and soft tissues as that calculated for bivalves (Mae *et al.*

2007; Dreier *et al.* 2012) and we extend it to brachiopods. We thus suggest that estimated soft tissue $\delta^{13}C_{org}$ values of our *Gigantoproductus* species might have varied from –32.0‰ to –28.9‰ and those of $\delta^{15}N_{org}$ from –1.0‰ to +5.1‰ (Fig. 10). These low values, and their wide range of variation, are within the range expected by organisms that host symbionts and that may have combined this strategy with suspension feeding (Mae *et al.* 2007; Dreier *et al.* 2012; Rossi *et al.* 2013). In fact, in the case of a strict suspension feeding strategy, we would have expected $\delta^{13}C_{org}$ soft tissue values at least higher than –27‰ (yellow field in Fig. 10), as $\delta^{13}C_{org}$ values documented for the Visean marine and terrestrial organic matter are respectively around –28‰ and –23‰, (Lewan 1980; Strauss & Peters-Kottig 2003), and there is an increase of 1‰ at each step in the trophic chain and there is at least one step from dietary carbon to suspension feeders. This is also supported by the slightly negative to slightly positive soft tissue $\delta^{15}N_{org}$ values, which are intermediate between known values of symbiotic animals and filter feeders. In particular, the intraspecific range of variation of $\delta^{15}N_{org}$ recorded by specimens of *G. inflatus* at Ricklow Quarry is similar to that reported by Rossi *et al.* (2013) for the mixotroph bivalve *Loripes lacteus* living at the edge rather than the inner parts of eelgrass meadows.

A comprehensive, detailed analysis of the possible explanations for gigantism in the Late Palaeozoic is beyond the scope of this study, but our data seem to suggest that the gigantic size reached by the species of *Gigantoproductus* could be the result of a mixotroph lifestyle, by which they could rely on the energy and nutrients derived both from endosymbiotic microbes and from filtered particulate food. These results, coupled with the high growth rates, exclude the 'gentle giant syndrome' for *Gigantoproductus* species**.**

Photosymbionts or chemosymbionts?

It is very difficult to speculate further if these large brachiopods hosted phototrophic or chemotrophic symbionts. However, there are several lines of evidence that make the first alternative more plausible: 1) the low $\delta^{13}C_{org}$/intermediate $\delta^{15}N_{org}$; 2) the massive calcite skeleton produced by the animal; and 3) the depositional environment.

The isotope values measured in the shell's organic matrix, and in particular the $\delta^{15}N_{org}$, which is considered the most robust proxy for the detection of ancient symbioses (see discussion above), seem to be more compatible with photosymbiosis than with chemosymbiosis. $\delta^{15}N_{org}$ is lower than expected for a filter-feeding strategy, but higher than for chemosymbiotic animals which usually show negative values (Nelson & Fisher

1995; Van Dover 2000; Mizota & Yamanaka 2003; Mae *et al.* 2007), although this may also be explained by a mixotroph strategy.

The biomineralization of the heavy exoskeleton of these *Gigantoproductus* species – which are not only large, but also very thick shelled - could have been aided by algal symbioses which led to removal of CO_2, facilitating the conversion from bicarbonate to carbonate and the growth of a thick columnar layer.

Finally, as shown in detail by Nolan *et al*. (2017), the Once-a-Week Quarry gigantoproductids were deposited in a high-energy setting. The gigantoproductid bed overlies cross-bedded crinoidal grainstone-rudstone accumulated in an inner ramp swept by currents. There is no clear evidence of palaeo-water depths, but the crinoidal grainstone-rudstone beds contain sparse specimens of putative red algae (*Ungdarella, Stacheia* and S*tacheoides*) and rare possible paleoberesellid fragments. The Ricklow Quarry gigantoproductid bed accumulated in a lower energy environment, below effective wave and current action within the shelter provided by relict mud mounds in middle ramp settings. The skeletal packstone deposits associated with the gigantoproductids contain sparse red algae (*Ungdarella*, *Fasciella* and *Stacheia*), abundant calcispheres, sparse to rare fragments of paleoberesellid algae and dasycladacean algae (*Koninkopora* and *Velebitella*, cf. Mamet & Roux 1975; Mamet 1991). The presence of algal fragments suggests that the water depths of deposition were within the photic zone in both settings, where the *Gigantoproductus* species may have exposed their photosymbionts to the light. There is no evidence of deviation from normal oxygen levels and the occurrence of a diverse fauna of associated crinoids, echinoids, benthic foraminifera (palaeotextularids, archaeidiscids, endothryrids, *Omphalotis*, *Globoendothyra*, *Pseudoendothyra*, *Tetrataxis*, *Tuberitina*, *Earlandia vulgaris*, *Bradyina*, *Valvulinella*, *Monotaxinoides*), fenestellid and fistuliporid bryozoans and corals indicates normal salinities.

The question is: Where could these animals have hosted their symbionts? We exclude the presence of symbionts in the lophophore arms, not only because there they could not have been exposed to the light, but mainly because the lophophore structure is simple and rudimentary, as discussed above. We may hypothesize that the symbionts were hosted in the mantle, as in Recent Tridacninae (Kirkendale & Paulay 2017). This may be supported by the life position of *Gigantoproducts* species, which are semi-infaunal and concave-convex, but have long trails raised well above the water-sediment interface, with the commissural plane more or less perpendicular to the plane of the substrate (Ferguson 1978; Angiolini *et al.* 2012). They were thus orthothetic as *Tridacna* and they may have

exposed their mantle with symbionts to light along the trail's edge. Furthermore, the anterior margin of the valves of the analysed species (and particularly of *G. inflatus*) is plicated by flutings (Pattison 1981), which lengthen the anterior commissure increasing the amount of mantle surface that can be exposed, as observed in some Tridacninae. Gigantoproductids may not have been alone in adopting alternative feeding strategies to promote large size and rapid growth. Apart from the lyttonioids and richthofenioids of the Permian (Cowen 1970), the large trimerellid brachiopods of the Ordovician and Silurian possibly possessed similar properties. These latter brachiopods probably grew aragonitic shells, since replaced by calcite. Nevertheless, in the giant *Gasconsia*, from the Katian rocks of the Oslo Region, 'warts' within the shell fabric were illustrated that were possibly generated around organic inclusions within the original shell (Hanken & Harper 1985).

In the geological record, some brachiopods have large shells (up to 10 cm) possibly obtained through methano- or thiotrophic diets, such as those of the superfamily Dimerelloidea, among which the Lower Cretaceous (late Hauterivian – Barremian) *Peregrinella* is the largest known Mesozoic rhynchonellid. It forms nearly monospecific shell concentrations in deep-water environments (e.g., Kiel *et al.* 2014). *Peregrinella* has a cosmopolitan distribution, but it was interpreted to be confined to ancient methane seep sites based on the geochemistry of the shell and the limestone host rock (e.g., Campbell & Bottjer 1995; Posenato & Morsilli 1999; Kiel *et al.* 2014). Isotope data suggest the occurrence of methanotrophic bacteria at seafloor seepage; however, it is not clear if *Peregrinella* was filter-feeding on bacterioplankton or had a symbiotic relationship (methanotrophy) with the microbes (Kiel *et al.* 2014). Other Palaeozoic and Mesozoic dimerelloids have been interpreted as having been associated with cold seeps and chemosynthetic environments, such as *Dzieduszyckia* (Devonian; Peckmann *et al.* 2007), *Ibergirhynchia* (Early Carboniferous; Gischler *et al.* 2003), *Halorella* (Late Triassic; Peckmann *et al.* 2011), and *Sulcirostra* (Early Jurassic; Peckmann *et al.* 2013). Among these, only the shell of *Dzieduszyckia* reached a large size similar to that of *Peregrinella,* but the shell size of the other dimerelloids is, however, in the range of a few centimetres. Also the Lower Jurassic *Anarhynchia* cf. *gabbi* has been related to hydrothermal vent deposits, with primary producers represented by chemoautotrophic bacteria that oxidize sulphides (Little *et al.* 1999).

CONCLUSIONS

A multidisciplinary approach, including palaeontology, size analysis, petrography, CL, SEM, EBSD, TEM, inorganic and organic stable isotope geochemistry, has been utilized to study species of *Gigantoproductus* from the Visean of Derbyshire, UK. We conclude that:

- a calcite-occluded organic fraction is preserved in the fossil shells, and its preserved amino acid composition is comparable with that observed in Recent brachiopod taxa;
- one of the possible explanation for the gigantic size and thick carbonate skeleton of these Palaeozoic benthic brachiopods could be a mixotroph lifestyle (indicated by the presence of amino acid), by which they could rely on the energy and nutrients derived both from photosymbiotic microbes and from filtered particulate food;
- $\delta^{13}C_{org}$ and $\delta^{15}N_{org}$ of the organic fraction can possibly be used to reconstruct models for feeding strategies in well preserved Palaeozoic brachiopods.

Acknowledgements.

We thank C. Malinverno (Milano) and A. Rizzi (Milano) for SEM support and analyses. L. Angiolini and G. Crippa acknowledge financial support of the 2011 Italian Ministry PRIN Project “Past ExcessCO2 worlds: biota responses to extreme warmth and ocean acidification” to E. Erba; D. Harper acknowledges support from the Leverhulme Trust (UK). A first version of the manuscript benefitted from reviews by an anonymous reviewer and E. Harper. M. H. Stephenson and M. J. Leng publish with permission of the CEO of the British Geological Survey.

DATA ARCHIVING STATEMENT

Additional photomicrographs and supplementary figures for this study are available in the Dryad Digital Repository: https://datadryad.org/review?doi=doi:10.5061/dryad.m42t6tm **[please note that the data for this paper are not yet published and this temporary link should not be shared without the express permission of the author]**

References

ANGIOLINI, L., DARBYSHIRE, D. P. F, STEPHENSON, M. H., LENG, M. J., BREWER, T. S., BERRA, F. and JADOUL, F. 2008. Lower Permian brachiopods from Oman: their potential as climatic proxies. *Earth and Environmental Science Transactions of the Royal Society of Edinburgh*, **98**, 3-4, 327–344

ANGIOLINI, L., JADOUL, F., LENG, M. J., STEPHENSON, M. H., RUSHTON, J., CHENERY, S., and CRIPPA, G. 2009. How cold were the Early Permian glacial tropics? Testing sea surface temperature using the oxygen isotope composition of rigorously screened brachiopod shells. *Journal of the Geological Society*, **166**, 933-945.

ANGIOLINI, L., STEPHENSON, M., LENG, M. J., JADOUL, F., MILLWARD, D., ALDRIDGE, A., ANDREWS, J., CHENERY, S. and WILLIAMS, G. 2012, Heterogeneity, cyclicity and diagenesis in a Mississippian brachiopod shell of palaeoequatorial Britain: *Terra Nova*, **24**, 1,16–26.

ANGIOLINI, L., CRIPPA, G., AZMY, K., CAPITANI, G., CONFALONIERI, G., DELLA PORTA, G., GRIESSHABER, E., HARPER, D.A.T., LENG, M.J., NOLAN, L., ORLANDI, M., POSENATO, R., SCHMAHL, W.W., BANKS, V.J., STEPHENSON, M.H. 2019. Data from: The giants of the phylum Brachiopoda: a matter of diet? *Dryad Digital Repository*. https://datadryad.org/review?doi=doi:10.5061/dryad.m42t6tm

ARMENDÁRIZ, M., ROSALES, I. and QUESADA, C. 2008. Oxygen isotope and Mg/Ca composition of Late Viséan (Mississippian) brachiopod shells from SW Iberia: Palaeoclimatic and palaeogeographic implications in northern Gondwana: *Palaeogeography, Palaeoclimatology, Palaeoecology*, **268**, 1–2, 65–79.

AZMY, K., KENDALL, B., BRAND, U., STOUGE, S. and GORDON, G. W. 2015. Redox conditions across the Cambrian–Ordovician boundary: Elemental and isotopic signatures retained in the GSSP carbonates. *Palaeogeography Palaeoclimatology Palaeoecology,* **440,** 440-454.

ARNAUD, P.M. 1974. Contribution à la bionomie marine benthique des régions antarctiques et subantarctiques. *Tethys,* **6**, 567–653.

BAUMGARTEN, S., LAUDIEN, J., JANTZEN, C., HÄUSSERMANN, V. and FÖRSTERRA, G. 2014. Population structure, growth and production of a recent brachiopod from the Chilean fjord region. *Marine Ecology*, **35**, 401–413-

BRUCKSHEN, P., OESMANN, S. and VEIZER, J. 1999. Isotope stratigraphy of the European Carboniferous. Proxy signals for ocean chemistry, climate and tectonics. *Chemical Geology*, **161**, 127-163.

BREISLIN, C. J. 2018. Basin-Scale Mineral and Fluid Processes at a Platform Margin, Lower Carboniferous, UK. PhD Thesis, University of Manchester

BRUNTON, C. H. C. 1982. The functional morphology and palaeoecology of the Dinantian brachiopod *Levitusia*. *Lethaia*, **15**, 149-167.

BUTLER, P. G., WANAMAKERJR., A. D., SCOURSE, J. D., RICHARDSON, C. A. and REYNOLDS, D. J. 2013. Variability of marine climate on the North Icelandic Shelf in a 1357-year proxy archive based on growth increments in the bivalve *Arctica islandica*. *Palaeogeography Palaeoclimatology Palaeoecology*, **373**, 141-151.

CAMPBELL, K. A. and BOTTJER, D. J. 1995. *Peregrinella*: an Early Cretaceous cold-seep-restricted brachiopod. *Paleobiology,* **21**, 461–478.

CASELLA, L. A., GRIESSHABER E., SIMONET RODA M., ZIEGLER A., MAVROMATIS V., HENKEL D., LAUDIEN J., HÄUSSERMANN V., NEUSER R. D., ANGIOLINI L., DIETZEL M., EISENHAUER A., IMMENHAUSER A., BRAND U. and SCHMAHL W. W. 2018a. Micro- and nanostructures reflect the degree of diagenetic alteration in modern and fossil brachiopod shell calcite: A multi-analytical screening approach (CL, FE-SEM, AFM, EBSD*). Palaeogeography, Palaeoclimatology, Palaeoecology*, **502**, 13–30.

CASELLA, L. A., SIMONET RODA, M. D. M., ANGIOLINI, L., ZIEGLER, A., SCHMAHL, W. W., BRAND, U. and GRIESSHABER, E. 2018b. Archival biogenic micro- and nanostructure data analysis: signatures of diagenetic systems, *Data In Brief*, **19**, 299–311

CUIF, J. P. 1972. Note sur des Madreporaires triasiques à fibres aragonitiques conservées. *Comptes rendus de l'Académie des Sciences*, **274**, 1272-1275.

CAVANAUGH, C. M., MCKINESS, Z. P., NEWTON, I. L. G. and STEWART, F. J. 2006. Marine chemosynthetic symbioses. 475-507. *In* DWORKIN, M., FALKOW, S., ROSENBERG, E. and STACKEBRANDT, E. (eds). *Prokaryotes. Volume 1: Symbiotic associations, Biotechnology, Applied Microbiology*. New York, N.Y. (Springer), 1012 pp.

CHÁVEZ-VILLALBA, J., LÓPEZ-TAPIA, M., MAZÓN-SUÁSTEGUI, J. and ROBLES-MUNGARAY, M. 2005. Growth of the oyster *Crassostrea corteziensis* (Hertlein, 1951) in Sonora, Mexico. *Aquaculture research*, **36**, 14, 1337-1344.

CHILDRESS, J. J. and FISHER, C. R. 1992. The biology of hydrothermal vent animals: physiology, biochemistry, and autotrophic symbioses. *Oceanography and Marine Biology – An Annual Review*, **30**, 337-441.

CLAYTON, R. N., O'NEIL, J. R. and MAYEDA, T. K. 1972. Oxygen isotope exchange between quartz and water. *Journal of Geophysical Research*, **77**, 17, 3057-3067.

COHEN, B. L., BITNER, M. A., HARPER, E., LEE, D. E., MUTSCHKE, E. and SELLANES, J. 2011. Vicariance and convergence in Magellanic and New Zealand long-looped brachiopod clades (Pan-Brachiopoda: Terebratelloidea). *Zoological Journal of the Linnean Society*, **162**, 631–645.

COWEN, R. 1970. Analogies between the Recent bivalve *Tridacna* and the fossil brachiopods Lyttoniacea and Richthofeniacea. *Palaeogeography, Palaeoclimatology, Palaeoecology*, **8**, 329-344.

COWEN, R. 1983. Algal symbiosis and ist recognition in the fossil record. 431-478. *In* TEVESZ M. J. S. MCCALL P.L. (eds). *Biotic interactions in recent and fossil benthic communities.* New York (Plenum), 812 pp.

COWEN, R. 1988. The role of algal symbiosis in reefs through time. *Palaios*, **3**, 221-227.

CRAIG, H. 1957. Isotopic standards for carbon and oxygen & correction factors for mass spectrometric analysis. *Geochemica et Cocmochemica Acta*, **12**, 133-149.

CURRY, G. B., ANSELL, A. D., JAMES, M. and PECK, L. 1989. Physiological constraints on living and fossil brachiopods. *Transactions of the Royal Society of Edinburgh: Earth Sciences*, **80**, 255–262.

CUSACK, M. and WILLIAMS, A. 2007. Biochemistry and Diversity of Brachiopod Shells. 2373-2395. *In* Selden, P.A. (ed.). *Treatise on Invertebrate Paleontology. Part H, Brachiopoda,* Revised*,* Volume 6: Supplement. Geological Society of America Inc., and The University of Kansas, Boulder, Colorado, USA, p. 2321-3226.

DALEY, R. L. and BOYD, D. W. 1996. The role of skeletal microstructure during selective silicification of brachiopods. *Journal of Sedimentary Research*, **66**, 1, 155-162.

DATTAGUPTA, S., BERGQUIST, D. C. and SZALAI, E. B. 2004. Tissue carbon, nitrogen, and sulfur stable isotope turnover in transplanted *Bathymodiolus childressi* mussels: relation to growth and physiological condition. *Limnology and Oceanography*, **49**, 4, 1144–1151.

DECOTTIGNIES, P., BENINGER, P. G., RINCÉ, Y. and RIERA, P. 2007. Trophic interactions between two introduced suspension-feeders, *Crepidula fornicata* and *Crassostrea gigas*, are influenced by seasonal effects and qualitative selection capacity. *Journal of Experimental Marine Biology and Ecology*, **342**, 2, 231-241.

DIXON, G. 1789. A voyage around the world; but more particularly to the north-west coast of America: performed in 1785, 1786, 1787, and 1788, in the King George and Queen Charlotte, Captains Portlock and Dixon: i-xxix + 1-360 + 1-48. London.

DREIER, A. and HOPPERT, M. 2014. Following the traces of symbiont bearing molluscs during earth history. 83–97. *In* WIESE, F., REICH, M. and ARP, G. (eds). *Spongy, slimy, cosy & more.* Commemorative volume in celebration of the 60th birthday of Joachim Reitner. Göttingen Contributions to Geosciences, **77,** 201 pp.

DREIER, A., STANNEK, L., BLUMENBERG, M., TAVIANI, M., SIGOVINI, M., WREDE, C., THIEL, V. and HOPPERT, M. 2012. The fingerprint of chemosymbiosis: origin and preservation of isotopic biosignatures in the nonseep bivalve *Loripes lacteus* compared with *Venerupis aurea*. *FEMS Microbiology Ecology*, **81**, 480-493.

DREIER, A., LOH, W., BLUMENBERG, M., THIEL, V., HAUSEREITNER, D. and HOPPERT, M. 2014. The isotopic biosignatures of photo- vs. thiotrophic bivalves: are they preserved in fossil shells? *Geobiology*, **12**, 5, 406-23.

DUPERRON, S, FIALA-MEDIONI, A., CAPRAIS, J. C., OLU, K. and SIBUET, M. 2007. Evidence for chemoautotrophic symbiosis in a Mediterranean cold seep clam (Bivalvia: Lucinidae): comparative sequence analysis of bacterial 16S rRNA, APS reductase and RubisCO genes. *FEMS Microbiology Ecology*, **59**, 64-70.

DUPLESSIS, M. R., DUFOUR, S. C., BLANKENSHIP, L. E., FELDBECK, H. and YAYANOS, A. A. 2004. Anatomical and experimental evidence for particulate feeding in *Lucinoma aequizonata* and *Parvilucina tenuisculpta* (Bivalvia: Lucinidae) from the Santa Barbara Basin. *Marine Biology*, **145**, 551-561.

EMIG, C. C. 1992. Functional disposition of the lophophore in living Brachiopoda. *Lethaia*, **25**, 291-302.

FERGUSON, J. 1978. Some aspects of the ecology and growth of the Carboniferous Gigantoproductids. *Proceedings of the Yorkshire Geological Society*, **42,** 41–54.

FOLK, R. L. and PITTMAN, J. S. 1971. Length-slow chalcedony: a new testament for vanished evaporites. *Journal of Sedimentary Research*, **41,** 4, 1045-1058.

FRANKOWIAK, K., MAZUR, M., GOTHMANN, A. M. and STOLARSKI, J. 2013. Diagenetic alteration of Triassic coral from the aragonite Konservat-Lagerstätte in Alakir Çay, Turkey: Implications for geochemical measurements. *Palaios,* **28**, 333–342.

FRY, B. 1988. Food web structure on Georges Bank from stable C, N, and S isotopic compositions. *Limnology and Oceanography,* **33**, 1182–1190.

GAFFEY, S.J. 1988. Water in skeletal carbonates. *Journal of Sedimentary Petr*ology, **58**, 397-414.

GARBELLI, C., ANGIOLINI, L., JADOUL, F. and BRAND, U. 2012. Micromorphology and differential preservation of upper Permian brachiopod low-Mg calcite. *Chemical Geology*, **298-299**, 1-10.

GARBELLI, C., ANGIOLINI, L., BRAND, U. and JADOUL, F. 2014. Brachiopod fabric, classes and biogeochemistry: implications for the reconstruction and interpretation of seawater carbon-isotope curves and records. *Chemical Geology*, **371**, 60-67.

GISCHLER, E., SANDY, M. R., PECKMANN, J. 2003. *Ibergirhynchia contraria* (F.A. Roemer, 1850), an Early Carboniferous seep-related rhynchonellide brachiopod from the Harz Mountains, Germany-a possible successor to *Dzieduszyckia*? *Journal of Paleontology,* **77**, 293–303.

GOETZ, A. J., STEINMETZ, D. R., GRIESSHABER, E., ZAEFFERER, S., RAABE, D., KELM, K., IRSEN, S., SEHRBROCK, A. and SCHMAHL, W. W., 2011. Interdigitating biocalcite dendrites form a 3-D jigsaw structure in brachiopod shells. *Acta Biomateralia,* **7**, 2237–2243.

GOLDSTEIN, R. H. 1986. Reequilibration of fluid inclusions in low temperature calcium-carbonate cement. *Geology***, 14**, 792–795.

GOLDSTEIN, R. H. 2001. Fluid inclusions in sedimentary and diagenetic systems. *Lithos***, 55**, 159–193.

GRIESSHABER, E., YIN, X., ZIEGLER, A., KELM, K., CHECA, A., EISENHAUER, A. and SCHMAHL, W. W., 2017. Patterns of mineral organization in carbonate biological hard materials. 245-272. *In* HEUSS-ASSBICHLER, S., AMTHAUER, G., JOHN, M. (eds). *Highlights in applied mineralogy*. De Gruyter, 344 pp.

GROSSMAN, E. L., MACLEOD, K. G., HOPPE, K. A. 1993. Evidence that inoceramid bivalves were benthic and harbored chemosynthetic symbionts: Comment and Reply. *Geology*, **21**, 1, 94-96.

GROSSMAN, E. L., YANCEY, T. E., JONES, T. E., BRUCKSCHEN, P., CHUVASHOV, B., MAZZULLO, S. J. and MII, H. S. 2008. Glaciation, aridification, and carbon sequestration in the Permo-Carboniferous: the isotopic record from low latitude. *Palaeogeography, Palaeoclimatology, Palaeoecology*, **268**, 222–233.

HANKEN, N. M. and HARPER, D. A. T. 1985. The taxonomy, shell structure, and palaeoecology of the trimerellid brachiopod *Gasconsia* Northrop. *Palaeontology,* **28,** 243-254.

HOLLIS, C. 1998. Reconstructing fluid history: an integrated approach to timing fluid expulsion and migration on the Carboniferous Derbyshire Platform, England. 153-159. *In* PARNELL, J. (ed.). *Dating and Duration of FluidFlow and Fluid-Rock Interaction*. Geological Society, London, Special Publications, **144**, 279 pp.

HOLLIS, C. and WALKDEN, G. 1996. The use of burial diagenetic calcite cements to determine the controls upon hydrocarbon emplacement and mineralization on a carbonate platform, Derbyshire, England. *Geological Society, London, Special Publications*, **107**, 1, 35-49.

Hollis, C. and Walkden, G., 2002. Reconstructing fluid expulsion and migration north of the Variscan Orogen, Northern England. *Journal of Sedimentary Research*, **72**, 5, 700-710.

IMMEL, F., GASPARD, D., MARIE, A., GUICHARD, M., CUSACK, M. and MARIN, F. 2015. Shell proteome of rhynchonelliform brachiopods. *Journal of Structural Biology,* **190**, 360–366.

JAKUBOWICZ, M., BERKOWSKI, B., CORREA, M. L., JAROCHOWSKA, E., JOACHIMSKI, M., and BELKA, Z. 2015. Stable isotope signatures of Middle Palaeozoic ahermatypic rugose corals–deciphering secondary alteration, vital fractionation effects, and palaeoecological implications. *PloS one*, **10**, 9, e0136289

JENNINGS, S. and WARR, K. J. 2003.Environmental correlates of large-scale spatial variation in the $\delta^{15}N$ of marine animals. *Marine Biology,* **142**, 1131-1140.

KELM, K., GOETZ, A., SEHRBROCK, A., IRSEN, S., HOFFMANN, R., SCHMALH W. W. and GRIESSHABER, E. 2012. Mosaic structure in the spines of *Holopneustes porossisimus*. *Zeitschrift für Kristallographie*, **227**, 758–765

KEY JR, M. M., WYSE JACKSON, P. N., HÅKANSSON, E., PATTERSON, W. P. and MOORE, M. D. 2005. Gigantism in Permian trepostomes from Greenland: testing the algal symbiosis hypothesis using ^{13}C and ^{18}O values. *Bryozoan studies* 2004, 141-151.

KIEL, S., GLODNY, J., BIRGEL, D., BULOT, L. G., CAMPBELL, K.A., GAILLARD, C., GRAZIANO, R., KAIM, A., LAZAR, I., SANDY, M. R. and PECKMANN, J. 2014. The Paleoecology, Habitats, and Stratigraphic Range of the Enigmatic Cretaceous Brachiopod *Peregrinella. PLoS ONE*, **9**, 10, e109260, 1-19.

KIRKENDALE, L. and PAULAY, G. 2017. Part N, Revised, Volume 1, Chapter 9: Photosymbiosis in Bivalvia. Treatise Online, **89**, 1–31.

KWAK, T. J. and ZEDLER, J. B. 1997. Food web analysis of southern California coastal wetlands using multiple stable isotopes. *Oecologia,* **110,** 2, 262–277.

LABARBERA, M. 1986. Brachiopd lophophores: functional diversity and scaling. 313-321. *In* RACHEBOEUF, P. R. and EMIG, C. C. (eds). *Le Brachiopodes fossiles et actuels. Biostratigraphie du Paleozoique*, Brest, 4, 500 pp.

LÉCUYER, C. and O'NEIL, J. R. (1994) Stable isotope compositions of fluid inclusions in biogenic carbonates. *Geochimica et Cosmochimica Acta*, **58**, 353-363.

LEE, J. J., MCENERY, N. E., KHAN, E. G. and SCHUSTER, F. 1979. Symbiosis and the evolution of larger foraminifera. *Micropalentology*, **25**, 118-140.

LEVIN, L. A. and MICHENER, R. H. 2002. Isotopic evidence for chemosynthesis-based nutrition of macrobenthos: The lightness of being at Pacific methane seeps. *Limnology and Oceanography*, **47**, 5, 1336–1345.

LEWAN, M. D. 1986. Stable carbon isotopes of amorphous kerogens from Phanerozoic sedimentary rocks. *Geochimica Cosmochimica Acta*, **50**, 1583–1591.

LITTLE, C. T. S., HERRINGTON, R. J., HAYMON, R. M. and DANELIAN, T. 1999. Early Jurassic hydrothermal vent community from the Franciscan Complex, San Rafael Mountains, California. *Geology*, **27**, 2, 167-–170.

LORRAIN, A., PAULET, Y-M., CHAUVAUD, L., SAVOYE, N., DONVAL, A. and SAOUT, C. 2002. Differential $\delta^{13}C$ and $\delta^{15}N$ signatures among scallop tissues: implications for ecology and physiology. *Journal of Experimental Marine Biology and Ecology,* **275**, 47-61.

MAE, A., YAMANAKA, T. and SHIMOYAMA, S. 2007. Stable isotope evidence for identification of chemosynthesis-based fossil bivalves associated with cold-seepages. *Palaeogeography, Palaeoclimatology, Palaeoecology,* **245**, 411-420.

MACKINNON, D. I. and LEE, D. E. 2006. Terebratelloidea. *In* KAESLER, R. L. (ed.). 2229-2244. *Treatise on Invertebrate Paleontology. Part H, Brachiopoda*. Revised, Volume 5: Rhynchonelliformea (part). Geological Society of America Inc., and The University of Kansas, Boulder, Colorado, USA, 1689-2320.

MALIVA, R. G. and SIEVER, R. 1988. Mechanism and controls of silicification of fossils in limestones. *The Journal of Geology*, **96**, 4, 387-398.

MAMET, B. and ROUX, A. 1975. Dasycladales dévoniennes et carbonifères de la Téthys occidentale. *Revista Española de Micropaleontología*, **7**, 2, 245-295.

MAMET, B. 1991. Carboniferous calcareous algae. 370-451.*In* RIDING, R (ed.). Calcareous algae and stromatolites. Springer, Berlin, Heidelberg, 561 pp.

MARINONI, N. and BROEKMANS, M. A. T. M. 2013. Microstructure of selected aggregate quartz by XRD, and a critical review of the crystallinity index. *Cement and Concrete Research*, **54**, 215–225.

MCCAMMON, H. M. 1973. The ecology of *Magellania venosa*, an articulate brachiopod. *Journal of Paleontology*, **47**, 266-278.

MCKINESS, Z. P., MCMULLIN, E. R., FISHER, C. R. and CAVANAUGH, C. M. 2005. A new bathymodioline mussel symbiosis at the Juan de Fuca hydrothermal vents. *Marine Biology*, **148**, 109–116.

MACLEOD, K. G. and HOPPE, K. A. 1992, Evidence that inoceramid bivalves were benthic and harbored chemosynthetic symbionts. *Geology*, **20**, 117-120.

MICHENER, R. H. and SCHELL, D. M. 1994. Stable isotope ratios as tracers in marine aquatic food webs.138–157. *In* LAJTHA, K. and MICHENER, R.H. (eds). *Stable Isotopes in Ecology and Environmental Science*. Oxford Blackwell Scientific Publications, London, 566 pp.

MINAGAWA, M. and WADA, E., 1984. Stepwise enrichment of ^{15}N along food chains: further evidence and the relation between $\delta^{15}N$ and animal age. *Geochimica Cosmochimica Acta*, **48**, 1135–1140.

MIZOTA, C. and YAMANAKA, T. 2003. Strategic adaptation of a deep-sea, chemosynthesis-based animal community: an evaluation based on soft body part carbon, nitrogen, and sulfur isotopic signatures. *Japanese Journal of Benthology*, **58**, 56–69 (in Japanese with English abstract).

MUIR-WOOD, H. M. and COOPER, G. A. 1960, Morphology, classification and life habits of the Productoidea (Brachiopoda). *Memoirs of the Geological Society of America*, **81**, 1–567.

MURATA, K. J. and NORMAN, M. B. 1976. An index of crystallinity for quartz. *American Journal of Science*, **276**, 1120-1130.

MURATA, K. J., FRIEDMAN, I. and GLEASON, J. D. 1977. Oxygen isotope relations between diagenetic silica minerals in Monterey Shale, Temblor Range, California. *American Journal of Science*, **277**, 3, 259-272.

MUSCATINE, L., GOIRAN, C., LAND, L., JAUBERT, J., CUIF, J. P. and ALLEMAND, D. 2005. Stable isotopes ($\delta^{13}C$ and $\delta^{15}N$) of organic matrix from coral skeleton. *Proceedings of the National Academy of Sciences*, **102**, 5, 1525-1530.

NELSON, D. C. and FISHER, C. R., 1995. Chemoautotrophic and Methanotrophic Endosymbiotic Bacteria at Deep-Sea Vents and Seeps.125–167. *In* KARL, D.M. (ed.). *The Microbiology of Deep-Sea Hydrothermal Vent Habitats*. CRC Press, Boca Raton.

NOLAN, L. S. P., ANGIOLINI, L., JADOUL, F., DELLA PORTA, G., DAVIES, S. J.,BANKS, V. J., STEPHENSON, M. H. and LENG, M. J. 2017. Sedimentary context and palaeoecology of *Gigantoproductus* shell beds in the Mississippian Eyam Limestone Formation, Derbyshire carbonate platform, central England. *Proceedings of the Yorkshire Geological Society*, **61**, 4, 239-257.

NOVACK- GOTTSHALL, P. M. 2006. Ecosystem-wide body-size trends in Cambrian – Devonian marine invertebrate lineages. *Paleobiology*, **34**, 210-228.

NOVACK-GOTTSHALL, P. M. and LANIER, M. A. 2008. Scale–dependence of Cope's rule in body-size evolution of Paleozoic brachiopods. *Proceedings of the National Academy of Sciences USA*, **105**, 5430-5434.

O'DONNELL, T. H., MACKO, S. A., CHOU, J., DAVIS-HARTTEN, K. L. and WEHMILLER, J. F. 2003. Analysis of $\delta^{13}C$, $\delta^{15}N$, and $\delta^{34}S$ inorganic matter from the biominerals of modern and fossil *Mercenaria* spp. *Organic Geochemistry*, **34**, 165-183.

ORME, G. R. 1973. Silica in the Visean limestones of Derbyshire, England. *Proceedings of the Yorkshire Geological Society*, **40**, 1, 63-104.

PALMER, A. R. 1999. Predator size, prey size, and the scaling of vulnerability: hatchling gastropods vs. barnacles. *Ecology*, **7**, 759-775.

PARK, Y.M., KO, D.S., YI, K.W., PETROV, I., KIM, Y.W. 2007. Measurement and estimation of temperature rise in TEM sample during ion milling. *Ultramicroscopy*, **107**, 663-668.

PATTISON, J. 1981.The stratigraphical distribution of gigantoproductoid brachiopods in the Visean and Namurian rocks of some areas of northern England. British Geological Survey Report CF81/09.

PAYNE, J. L., HEIM, N. A., KNOPE, M. L. and MCCLAIN, C. R. 2014. Metabolic dominance of bivalves predates brachiopod diversity decline by more than 150 million years. *Proceedings of the Royal Society B, Biological Sciences*, **281**, 2013.3122

PECK, L. S. 1996. Metabolism and feeding in the Antarctic brachiopod *Liothyrella uva*: a low energy lifestyle species with restricted metabolic scope. *Proceedings of the Royal Society B, Biological Sciences*, **263**, 1367, 223-228.

PECKMANN, J., CAMPBELL, K. A., WALLISER, O. H., REITNER, J. 2007. A Late Devonian hydrocarbon-seep deposit dominated by dimerelloid brachiopods, Morocco. *Palaios,* **22**, 114–122.

PECKMANN, J., KIEL, S., SANDY, M.R., TAYLOR, D.G. and GOEDERT, J.L. 2011. Mass occurrences of the brachiopod *Halorella* in Late Triassic methane-seep deposits, eastern Oregon. *Journal of Geology*, **119**, 207–220.

PECKMANN, J., SANDY, M. R., TAYLOR, D. G., GIER, S. and BACH, W. 2013. An Early Jurassic brachiopod-dominated seep deposit enclosed by serpentinite, eastern Oregon, USA. *Palaeogeography, Palaeoclimatology, Palaeoecology,* **390**,4–16.

PEREIRA, A. A., VAN HATTUM, B., DE BOER, J., VAN BODEGOM, P. M., REZENDE C. E. and SALOMONS, W. 2010. Trace Elements and Carbon and Nitrogen Stable Isotopes

in Organisms from a Tropical Coastal Lagoon. *Archives of Environmental Contamination and Toxicology*, **59**, 464–477.

PILE, A. J. and YOUNG, C. M. 1999. Plankton availability and retention efficiencies of cold-seep symbiotic mussels. *Limnology Oceanography*, **44**, 7, 1833–1839.

POPP, B. N., ANDERSON, T. F. and SANDBERG, P. A. 1986. Brachiopods as indicators of original isotopic compositions in some Paleozoic limestones. *Geological Society of America Bulletin*, **97**, 1262–1269.

POSENATO, R. and MORSILLI, M. 1999. New species of *Peregrinella* from the Lower Cretaceous of the Gargano Promontory (Southern Italy). *Cretaceous Research*, **20**, 641–654.

QIAO, L., and SHEN, S. Z. 2015. A global review of the Late Mississippian (Carboniferous) *Gigantoproductus* (Brachiopoda) faunas and their paleogeographical, paleoecological, and paleoclimatic implications. *Palaeogeography, Palaeoclimatology, Palaeoecology*, **420**, 128–137.

RAU, G. H. and HEDGES, J. I. 1979. Carbon-13 depletion in a hydrothermal vent mussel: suggestion of a chemosynthetic food source. *Science,* **203**, 16, 648–649.

ROBINSON, J. J. and CAVANAUGH, C. M. 1995. Expression of form I and form II Rubisco in chemoautotrophic symbioses: Implications for the interpretation of stable carbon isotope values. *Limnology and Oceanography*, **40**, 1496-1502.

RODRIGUEZ-NAVARRO, C., RUIZ-AGUDO, E., LUQUE, A., RODRIGUEZ-NAVARRO, A.B. and ORTEGA-HUERTAS, M. 2009. Thermal decomposition of calcite: Mechanisms of formation and textural evolution of CaO nanocrystals. *American Mineralogist,* **94**, 578–593.

ROSA, R. and SEIBEL, B. A. 2010. Slow pace of life of the Antarctic colossal squid. *Journal of the Marine Biological Association of the United Kingdom*, **90**, 375–378.

ROLLION-BARD, C., BLAMART, D., CUIF, J. P. and JUILLET-LECLERC, A. 2003. Microanalysis of C and O isotopes of azooxanthellate and zooxanthellate corals by ion microprobe. *Coral Reefs*, **22**, 4, 405-415.

ROSSI, F., COLACO, E., MARTINEZ, M. J., KLEIN, J. C., CARCAILLET, F., CALLIERE M. D., DE WIT, R. and CARO, A. 2013. Spatial distribution and nutritional requirements of the endosymbiont-bearing bivalve *Loripes lacteus* (sensu Poli, 1791) in a Mediterranean *Nanozostera noltii* (Hornemann) meadow. *Journal of Experimental Marine Biology and Ecology*, **440**, 108-115.

RUSH, P. F. and CHAFETZ, H. S. 1990. Fabric retentive, non–luminescent brachiopods as indicators of original $\delta^{13}C$ and $\delta^{18}O$ compositions: a test. *Journal of Sedimentary Petrology,* **60**, 968–981.

SARYTCHEYA, T.G. 1928. The Productidae of the group *Productus giganteus* Mart. from the Visean of Moscow. Memorandum of the Geological Science Research Institute. Physics and Maths Faculty. 1st Moscow State University, 1, 71.

SCHLESER, G. H., FRIELINGSDORF, J. and BLAIR, A. 1999. Carbon isotope behaviour in wood and cellulose during artificial aging. *Chemical Geology*, **158**, 121–130.

SCHMAHL, W. W., GRIESSHABER, E., KELM, K., GOETZ, A., JORDAN, G., BALL, A., XU, D., MERKEL, C. and BRAND, U. 2012. Hierarchical structure of marine shell biomaterials: biomechanical functionalization of calcite by brachiopods. *Zeitschrift für Kristallographie – Crystalline Materials*, **227**, 793–804.

SCHMITT, J. G. and BOYD, D. W. 1981. Patterns of silicification in Permian pelecypods and brachiopods from Wyoming. *Journal of Sedimentary Research*, **51**, 4, 1297-1308.

SHIINO, Y. and KUWAZURU, O. 2011. Theoretical approach to the functional optimization of spiriferide brachiopod shell: Optimum morphology of sulcus. *Journal of Theoretical Biology*, **276**, 192–198.

SHIINO, Y. and SUZUKI, Y. 2011. The ideal hydrodynamic form of the concavo-convex productide brachiopod shell. *Lethaia*, **44**, 329–343.

SMITH, A. C., KENDRICK, C. P., MOSS-HAYES, V. L., VANE, C. H., and LENG, M. J. 2017. Carbon isotope alteration during the thermal maturation of non-flowering plant species representative of those found within the geological record. *Rapid Communications in Mass Spectrometry*, **31**, 21–26. SORAUF, J. E. 1999. Skeletal microstructure, geochemistry, and organic remnants in cretaceous scleractinian corals: Santonian Gosau beds of Gosau, Austria. *Journal of Paleontology*, **73**, 1029–1041.

STANLEY, G. D. and SWART, P. K. 1995. Evolution of the coral-zooxanthellae symbiosis during the Triassic: a geochemical approach. *Paleobiology*, **21**, 2, 179-199.

STRAUSS, H. and PETERS-KOTTIG, W. 2003. The Paleozoic to Mesozoic carbon cycle revisited: the carbon isotopic composition of terrestrial organic matter. *Geochemistry, Geophysics, Geosystems*, **4**, 1-15.

TORNABENE, C., MARTINDALE, R. C., WANG, X. T. and SCHALLER, M. F. 2017. Detecting photosymbiosis in fossil scleractinian corals. *Scientific reports*, **7**, 1, 9465.

VANDENBROUCKE, M. and LARGEAU, C. 2007. Kerogen origin, evolution and structure. *Organic Geochemistry*, **38**, 719–833.

VAN DOVER, C. L. 2000. The Ecology of Deep-Sea Hydrothermal Vents. Princeton University Press, New Jersey, p. 424.

VEIZER, J., ALA, D., AZMY, K., BRUCKSCHEN, P., BUHL, D., BRUHN, F., CARDEN, G. A. F., DIENER, A., EBNETH, S., GODDERIS, Y., JASPER, T., KORTE, C., PAWELLEK, F., PODLAHA, O. G. and STRASS, H. 1999. 87Sr/86Sr, δ18O and δ13C evolution of Phanerozoic seawater. *Chemical Geology*, **161**, 59-88.

VERMEIJ, G. J. 2012. The evolution of gigantism on temperate seashores. *Biological Journal of the Linnean Society*, **106**, 776-793

VERMEIJ, G. J. 2016. Gigantism and its Implications for the history of Life. *PLoS ONE*, **11**, 1, e0146092. doi:10.1371/journal.pone.0146092

VOGEL, K. 1975. Endosymbiotic algae in rudists? *Palaeogeography, Palaeoclimatology, Palaeoecology*, **17**, 327-332.

WILLIAMS, A. and CUSACK, M. 2007. Chemicostructural diversity of the brachiopod shell. 2396-2521. *In* Selden, P.A. (ed.). *Treatise on Invertebrate Paleontology. Part H, Brachiopoda*. Revised, Volume 6: Supplement. Geological Society of America Inc., and The University of Kansas, Boulder, Colorado, USA, p. 2321-3226.

YAMAZAKI, A., WATANABE, T., TAKAHATA, N., SANO, Y. and TSUNOGAI, U. 2013. Nitrogen isotopes in intra-crystal coralline aragonites. *Chemical Geology*, **351**, 276–280.

YE, F., CRIPPA, G., ANGIOLINI, L., BRAND, U., CAPITANI, G., CUSACK, M., GARBELLI, C., GRIESSHABER, E., HARPER, E. M. and SCHMAHL W. W. 2018a. Mapping of recent brachiopod microstructure: A tool for environmental studies. *Journal of Structural Biology*, **201**, 3, 221-236.

YE, F., CRIPPA, G., GARBELLI, C. and GRIESSHABER, E. 2018b. Microstructural data of six recent brachiopod species: SEM, EBSD, morphometric and statistical analyses. *Data in Brief*, **18**, 300–318.

YE, F., JURIKOVA, H., ANGIOLINI, L., BRAND, U, CRIPPA, G., HENKEL, D., LAUDIEN, J., HIEBENTHAL, C., and ŠMAJGL, D. 2019. Variation in brachiopod microstructure and isotope geochemistry under low-pH–ocean acidification conditions. *Biogeosciences*, **16**, 617–642.

ZHANG, Z., AUGUSTIN, M. and PAYNE, J. L. 2015. Phanerozoic trends in brachiopod body size from synoptic data. *Paleobiology*, **41,** 3, 491-501.

FIGURE CAPTION

Fig. 1. Geological sketch map (from Nolan *et al.* 2017). A, The location of the Derbyshire carbonate platform (DCP) within mainland Great Britain. B, Outline of the platform with outcrop of Mississippian formations indicated. Sites: Ricklow Quarry (53.192N, 1.755W), Once-a-Week Quarry (53.209N, 1.766W), Ible (53.111N, 1.630W), Wensley Dale (53.146N, 1.608W). On the right: Derbyshire carbonate platform stratigraphy of the Peak Limestone Group: on-shelf (right) and off-shelf (left) provinces with regional chronostratigraphy. Key: M, carbonate mud–mounds; SB, Stanton Basin with eastern margin marked with the dashed line along with the Taddington–Bakewell Anticline and the Cronkston-Bonsall Fault; SS, Stanton syncline.

Fig. 2. A, and B, Photomicrographs under parallel and crossed polarizers of the ventral valve showing patches of silicification as spherulitic chalcedony only at the inner (top) and outer (bottom) margins of the columnar tertiary layer (specimen OAW203; scale bar 2 mm). C, Close-up view of the two types of silica replacement: spherulitic fibrous chalcedony on the upper right and euhedral quartz on the bottom left following the fibrous chalcedony (image in crossed polarizers, specimen OAW105b; scale bar 2 mm). D, The dorsal valve (in the centre) is often affected by silica replacement in both the inner and outer margins whereas the ventral valve (left side of image) appears pristine (specimen OAW8; scale bar 3 mm). E, Silicification on the outer margin of the dorsal valve affected by a stylolite suggesting that silica replacement took place early, during diagenesis before pressure solution (specimen RCK11; scale bar 1 mm). F, Silicification on the outer margin of the dorsal valve crossed by a fracture filled by burial diagenesis calcite (specimen OAW105; scale bar 1 mm).

Fig. 3. A, and B, Photomicrographs under parallel polarizers (A) and cathodoluminescence (B) of the specimen *G. inflatus* show that the ventral valve (below) is largely non luminescent except the outer margin of the columnar layer at the boundary with the laminar layer (often not present) where chalcedony spherulites occur and along some growth lines. The dorsal valve (above) shows evidence of skeletal calcite recrystallization substituted by luminescent equant sparite. The peloidal skeletal packstone-wackestone sediment in between the valves displays a blotchy luminescence (specimen RCK41 oriented with the outer margin of ventral valve at the bottom of the image; scale bar 1 mm). C, and D, Photomicrographs under parallel polarizers (C) and cathodoluminescence (D) of the outer margin of the columnar layer of the ventral valve showing non luminescent chalcedony spherulites surrounded by luminescent calcite that represents the altered outer portion of the tertiary layer adjacent to non altered columnar crystals towards the middle

portion of the valve (towards the right), except along the crystal boundaries (specimen OAW209; scale bar 1 mm). E, and F, Photomicrographs under parallel polarizers (E) and cathodoluminescence (F) of the columnar tertiary layer cut by a fracture filled by dull luminescent calcite followed by euhedral rhombic dolomite crystals which have an euhedral non luminescent nucleus overgrown by a luminescent growth phase (specimen RCK35; scale bar 1 mm).

Fig. 4. SEM photomicrographs showing shell microstructure. A, laminar secondary layer with pseudopunctae, *G. inflatus* (specimen OAW3; scale bar 200 μm). B, intercalation of laminar secondary layer and columnar tertiary layer; the transition between the fabrics is well preserved, *G. inflatus* (specimen RCK300; scale bar 100 μm). C, well preserved columnar tertiary layer with stepped growth lines inside the columns, *G. inflatus* (specimen OAW3; scale bar 200 μm). D, details of stepped growth lines inside the columns, *G. inflatus* (specimen RCK35; scale bar 20 μm). E, silicification as spherulitic chalcedony in the outer part of the shell, *G. okensis* (specimen RCK36; scale bar 500 μm). F, Detail of the growth of euhedral megaquartz crystals overgrowing chalcedony spherulites within the columnar tertiary layer, *G. inflatus* (specimen OAW212; scale bar 100 μm). These outer parts of the columnar layer were not sampled for geochemical analyses.

Fig. 5. TEM images of specimen RCK16. A, selected area diffraction pattern of calcite along the <1-1 0> direction showing the c-axis oriented parallel to the section plane. B, bright field image showing an ovoidal inclusion where a crystalline precipitate, an amorphous material (fluid, gel, glass) and a void, possibly filled by a gas, are visible (scale bar 50 nm). C, ovoidal inclusions with euhedral crystalline precipitates (scale bar 100 nm).

Fig. 6. TEM bright field images of specimen RCK16. A, inclusions interconnected by dislocations (arrows; scale bar 50 nm). B, inclusion trail along a dislocation (scale bar 100 nm). C, nanosized inclusions along calcite grain boundary (intergranular organics; scale bar 50 nm).

Fig. 7. EBSD images. A**,** EBSD band contrast (1) and orientation (2) measurement images with corresponding pole figures of a shell portion of *G. elongatus* (OAW203). Large columnar units of the tertiary layer form the shell, with calcite crystallite being highly co-oriented, thus, not altered by diagenetic overprint. B**,** EBSD band contrast (1) and orientation (2) measurement images with corresponding pole figures of a shell portion of *G. inflatus* (RCK221). The specimen is not altered as calcite co-orientation is high (see pole figures for calcite c- and a-axes) and the columnar microstructure characteristic of the tertiary layer is well preserved. C, EBSD band contrast (1) and orientation (2)

measurement images with corresponding pole figures of a shell portion of *G. okensis* (RCK16). According to differences in microstructure (Figure B, compare shell portions highlighted with black and blue rectangle) we can clearly distinguish between overprinted and pristine or very little disturbed shell portions. Unaltered or slight altered portions of the tertiary layer show the original biogenic microstructure (blue rectangle in 2) as well as a tight coherence of calcite crystallite c- and a*axes (3). In contrast, in the overprinted secondary layer (black rectangle in 2), the biogenic microstructure is entirely erased by newly formed calcite, the latter crystallized with a random orientation pattern (4).

Fig. 8. ^{1}H-NMR analysis. A, cluster at 1.90, 1.70, 1.45 ppm typical of amino acid aliphatic chain such as alanine, leucine or isoleucine. B, cluster at 2.9 e 2.80 ppm referring to lateral chain of aspartate/asparagine.

Fig. 9. Internal characters of *Gigantoproductus*. The specimen on the right is a composite fossil showing the ventral valve thickness, part of the ventral valve internal mould (with mould of brachial cones) and part of the interior of the dorsal valve with brachial ridges (modified from Angiolini *et al.* 2012).

Fig. 10. $\delta^{13}C_{org}$ - $\delta^{15}N_{org}$ plot showing the measured isotope values for the shell's organic matrix (orange and grey dots) and the reconstructed isotopic composition of soft tissues (arrows to red and blue dots) of the investigated species of *Gigantoproductus*, based on a bivalve model. $\delta^{13}C_{org}$ values for Visean organic and terrestrial matter are reported from the literature (their $\delta^{15}N_{org}$ values are not known) (Lewan 1980; Strauss & Peters-Kottig 2003). The yellow field represents theoretical values of $\delta^{13}C_{org}$ for the soft tissues of species pursuing a strict suspension feeding strategy and is calculated considering an increase of 1‰ relative to dietary carbon at each step-wise increase in trophic level (O'Donnel *et al.* 2003). See text for discussion.

Table 1. Width, length (mm) and log-transformed shell area of 50 specimens of *G. elongatus*, *G. inflatus* and *G. okensis* (1A) and of 69 specimens of species of other brachiopod genera (1B) from the Visean Monsal Dale Limestone and Eyam Limestone formations of Ible, Wensley Dale, Once-a-week and Ricklow quarries.

Table 2. SEM and cathodoluminescence screening and stable oxygen and carbon isotope composition of the calcite of the shell of *Gigantoproductus* species.

Table 3. Carbon and nitrogen isotopes from the organic fractions isolated from the shell calcite.

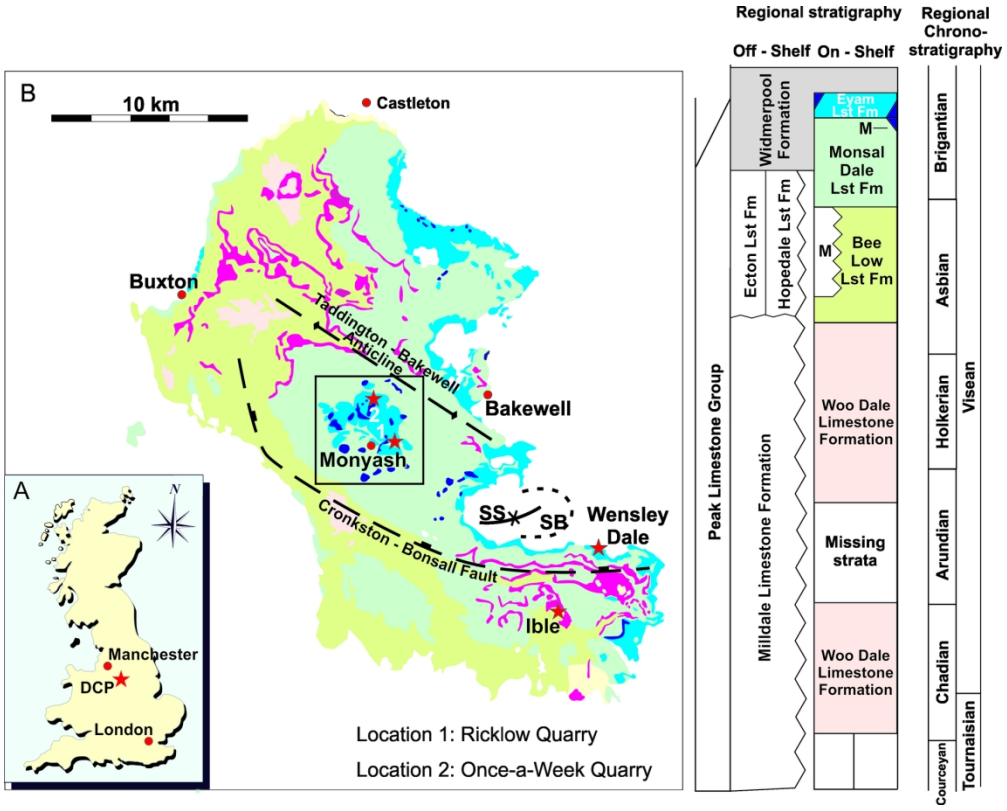

Figure 1

166x132mm (300 x 300 DPI)

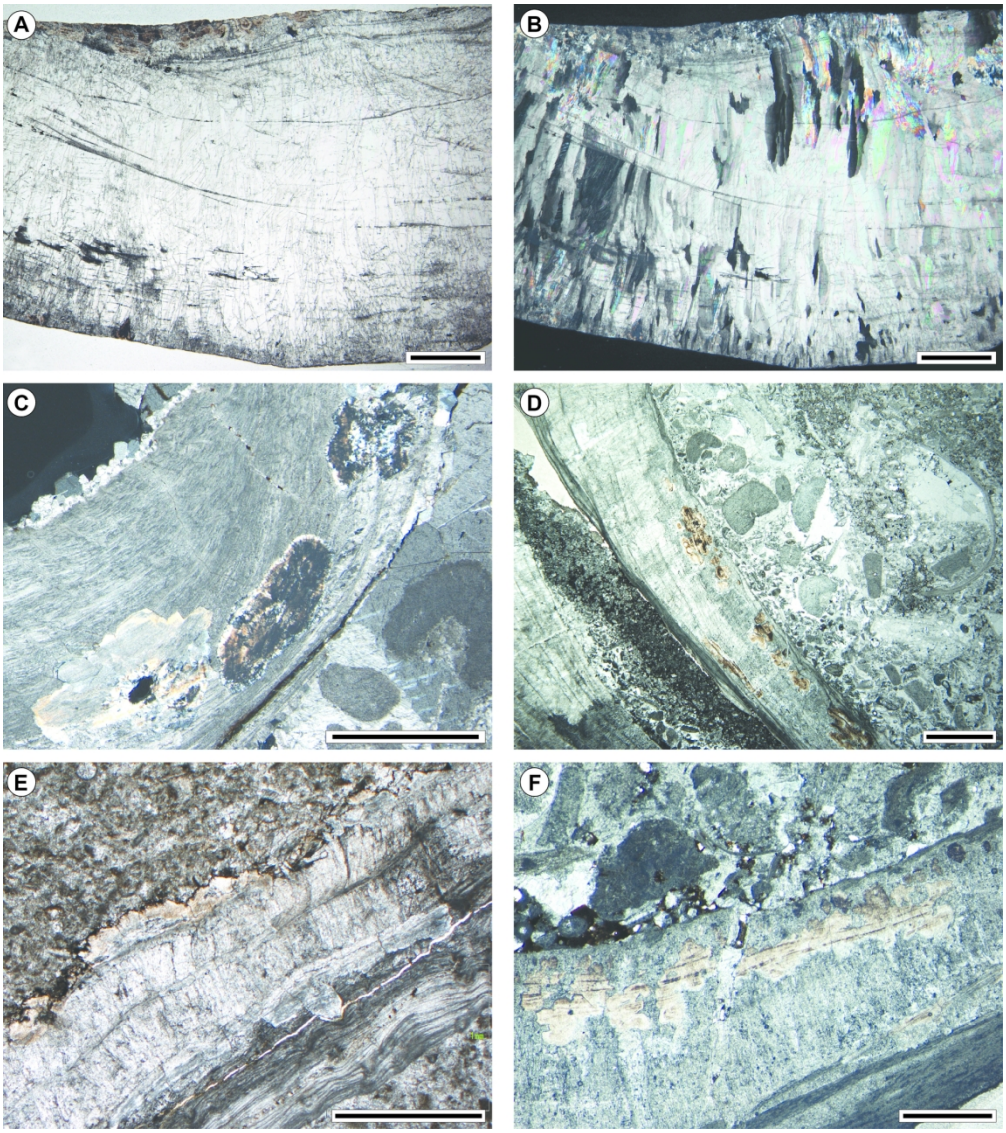

Figure 2

159x179mm (300 x 300 DPI)

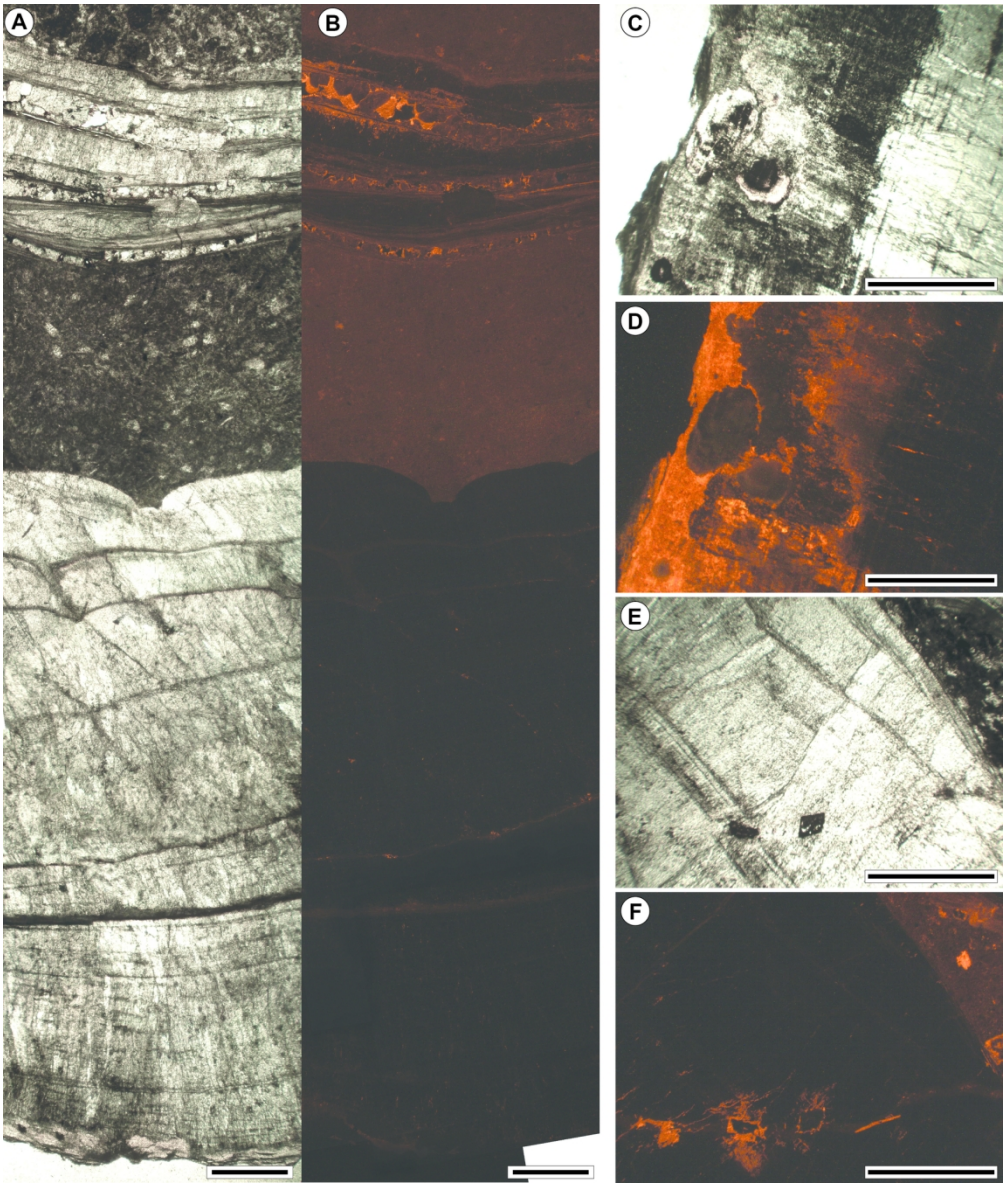

Figure 3

157x185mm (300 x 300 DPI)

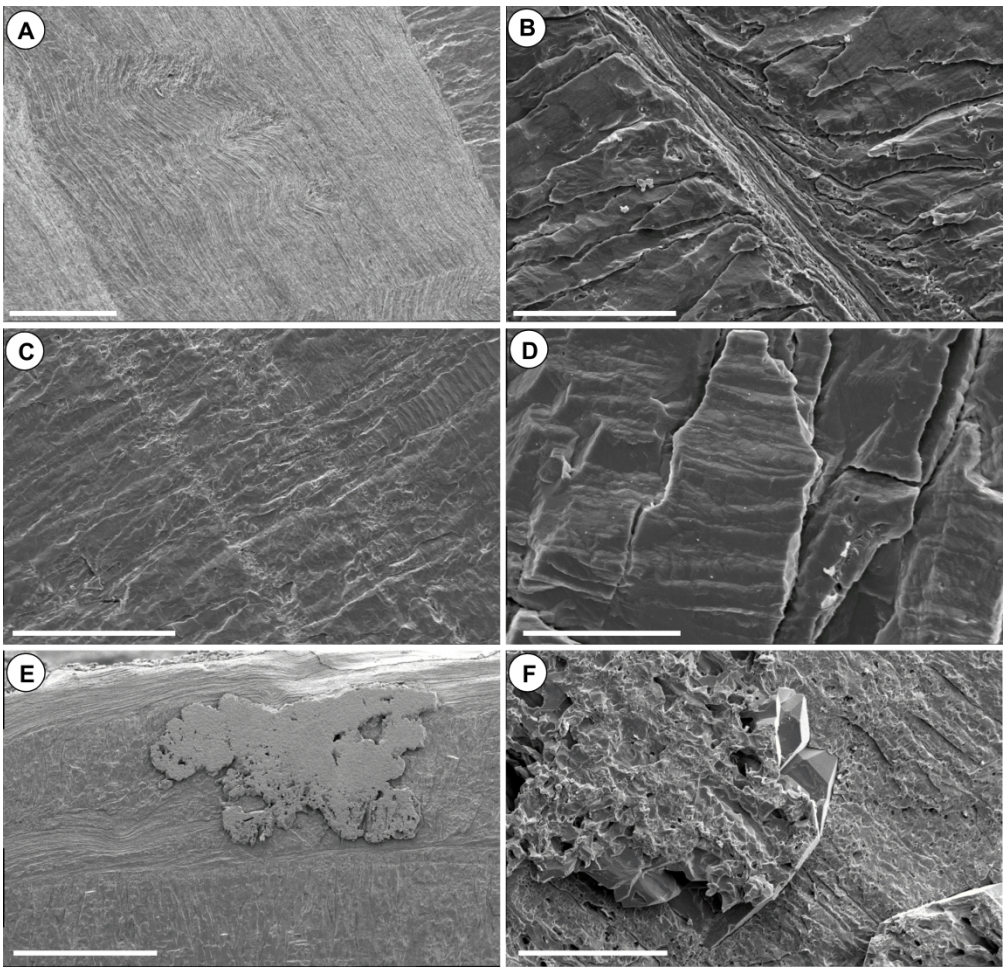

Figure 4

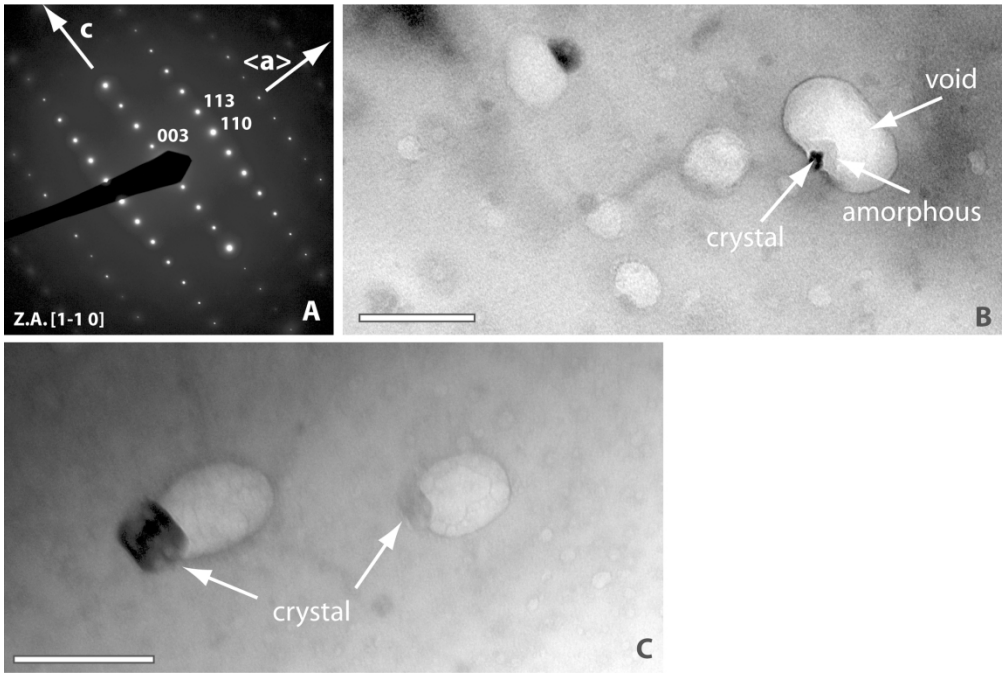

Figure 5

204x136mm (300 x 300 DPI)

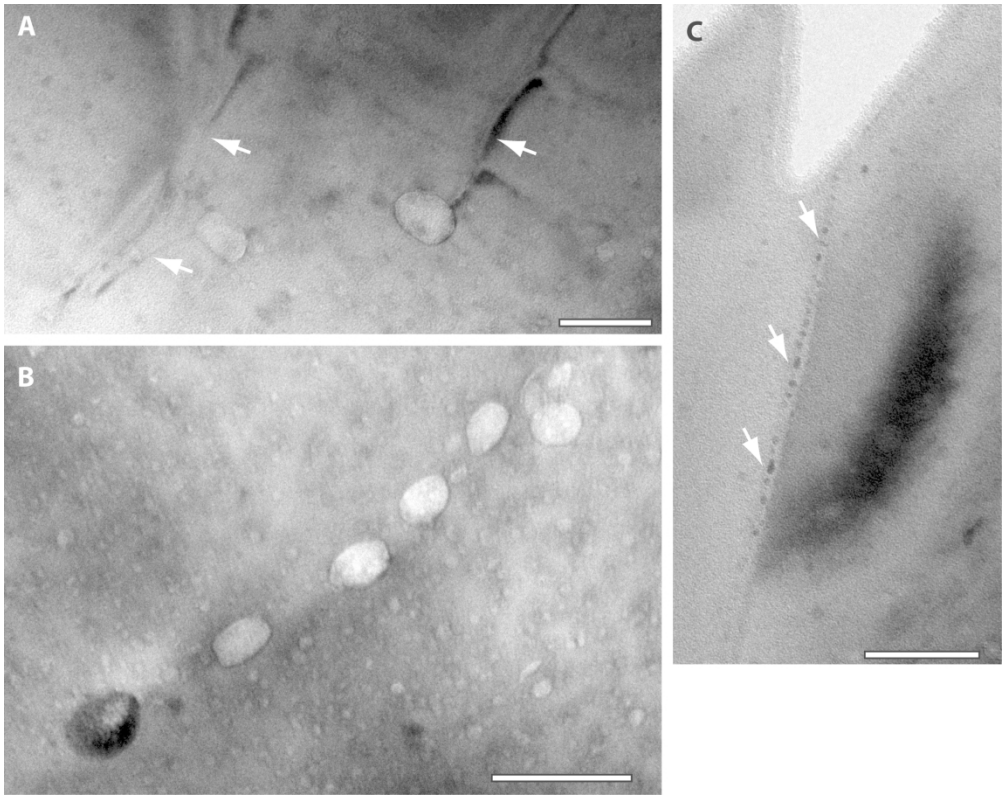

Figure 6

206x162mm (300 x 300 DPI)

A

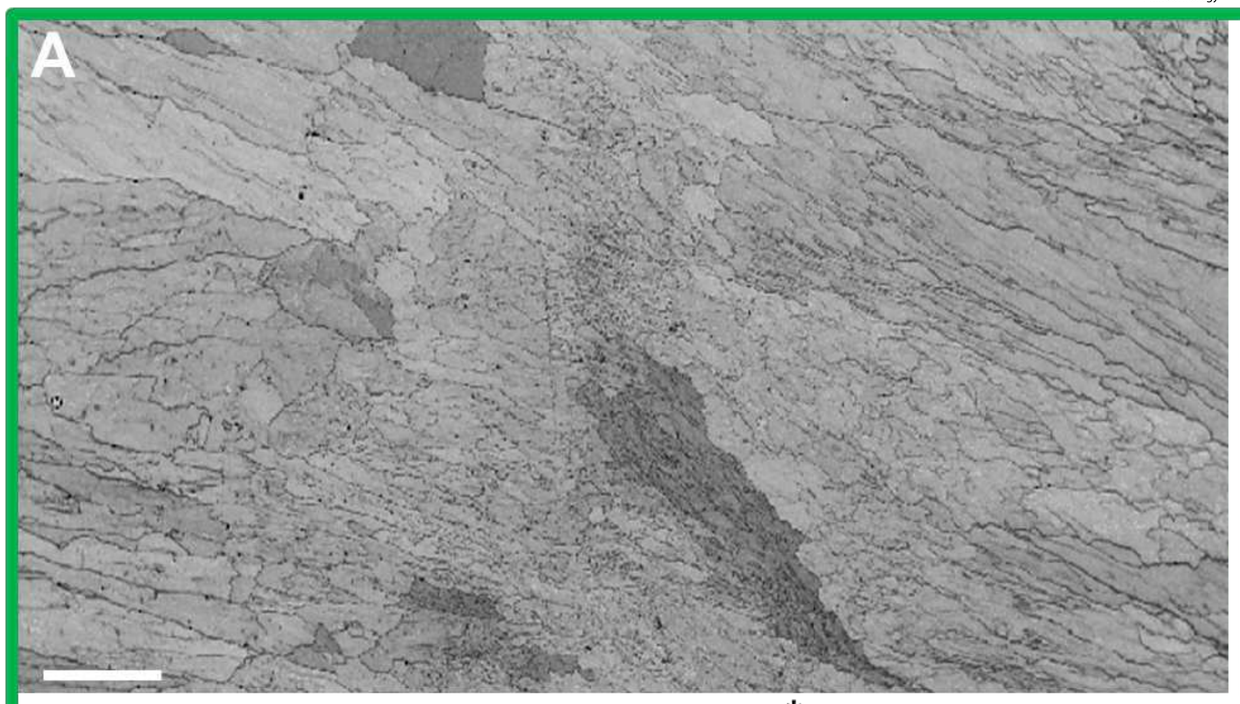
A

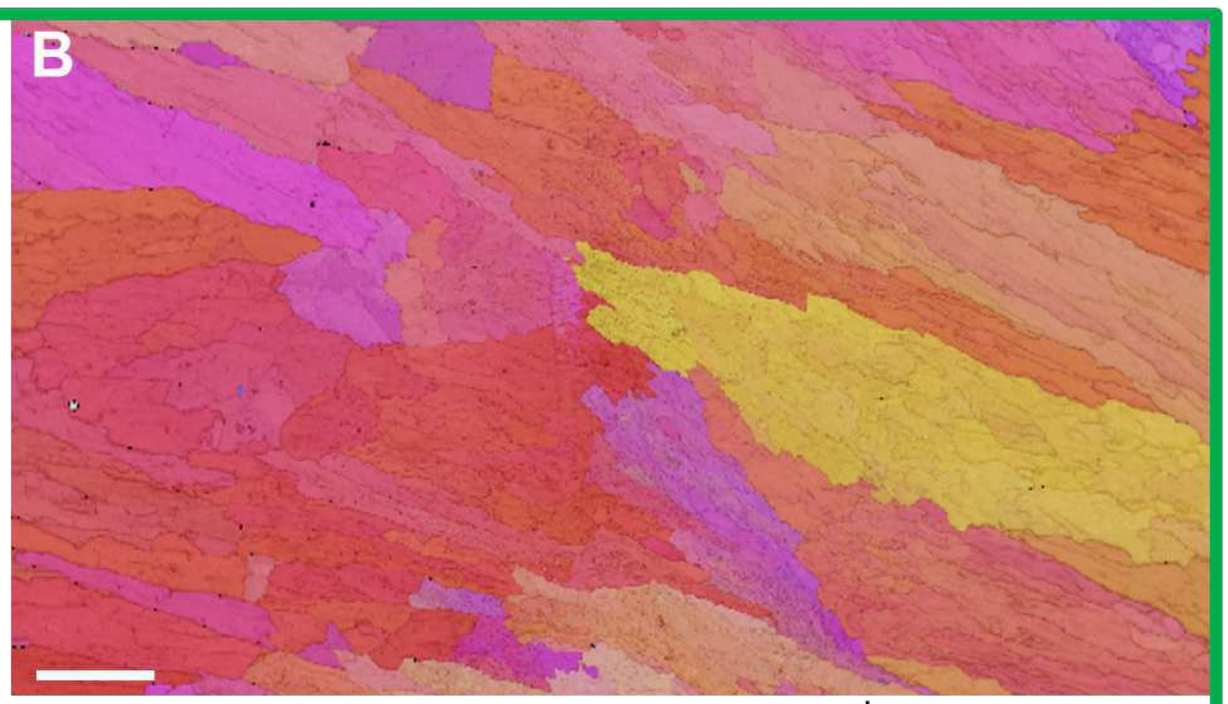
B

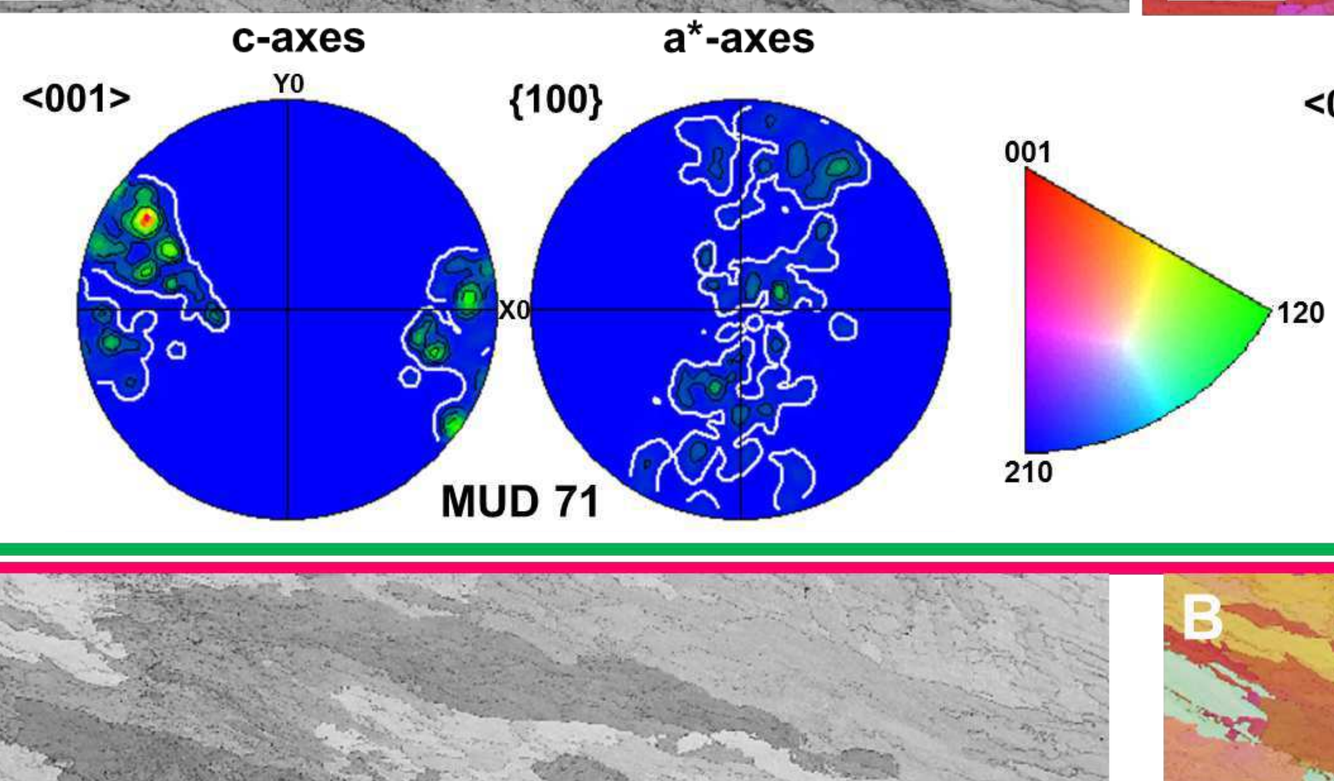
c-axes
a*-axes
<001>
Y0
{100}
X0
001
120
210
C
MUD 71

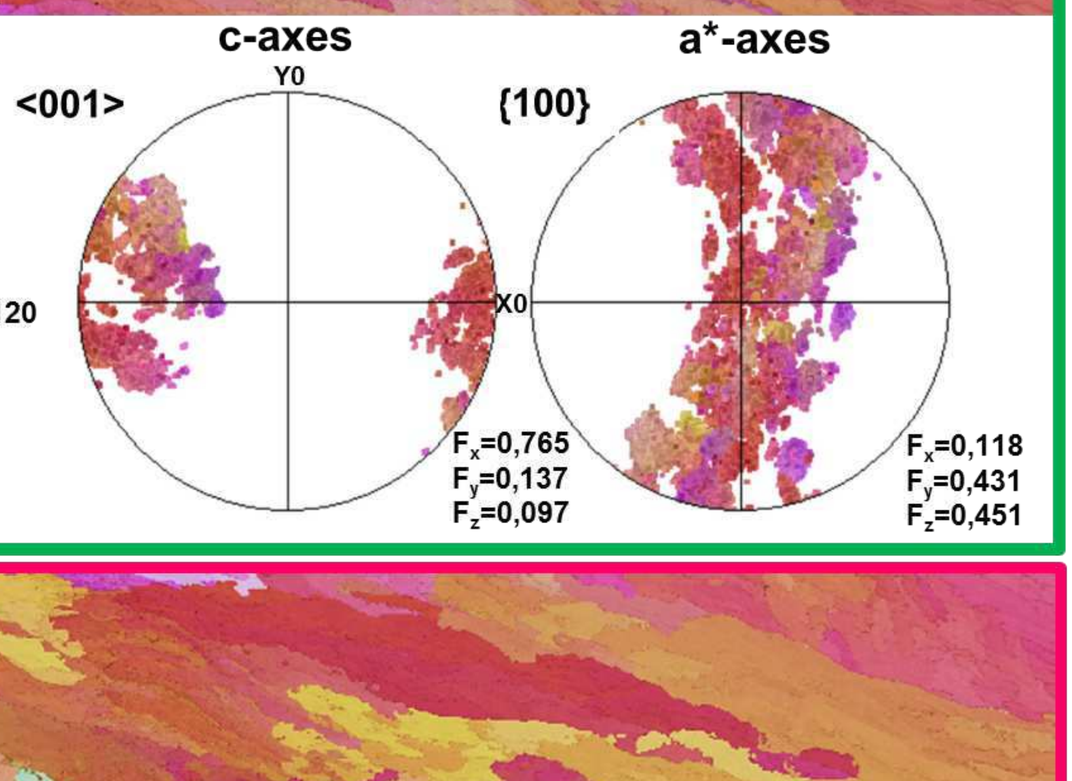
c-axes
a*-axes
<001>
Y0
{100}
X0
Fx=0,765
Fy=0,137
Fz=0,097
Fx=0,118
Fy=0,431
Fz=0,451

B


A


B

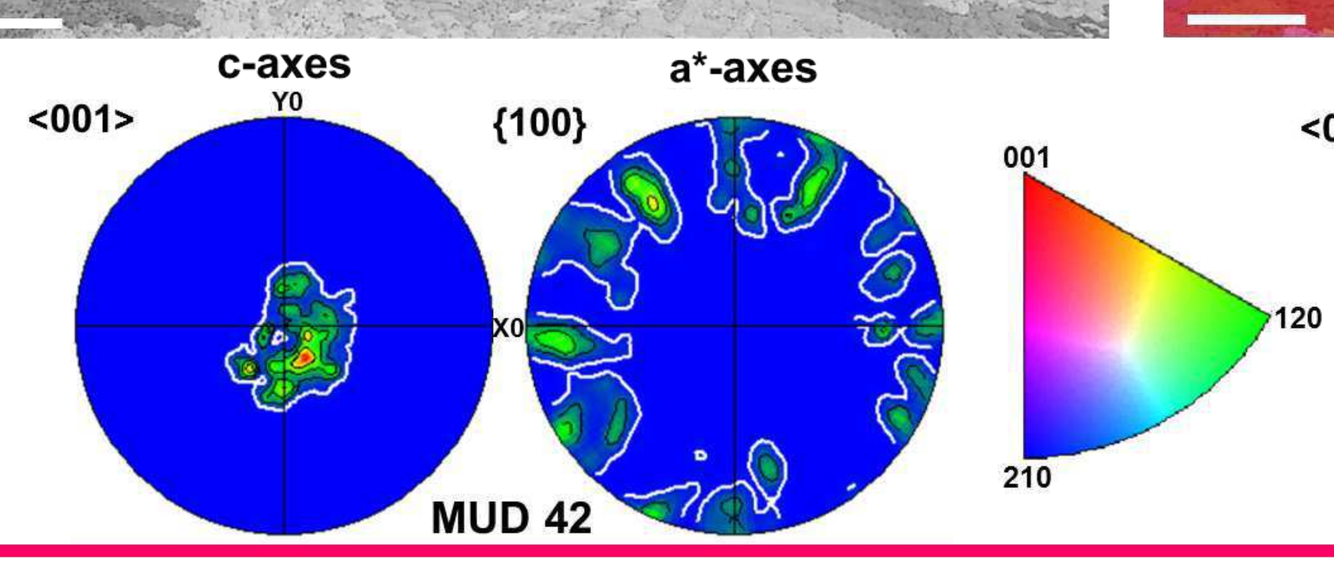
c-axes
a*-axes
<001>
Y0
{100}
X0
001
120
210
C
MUD 42

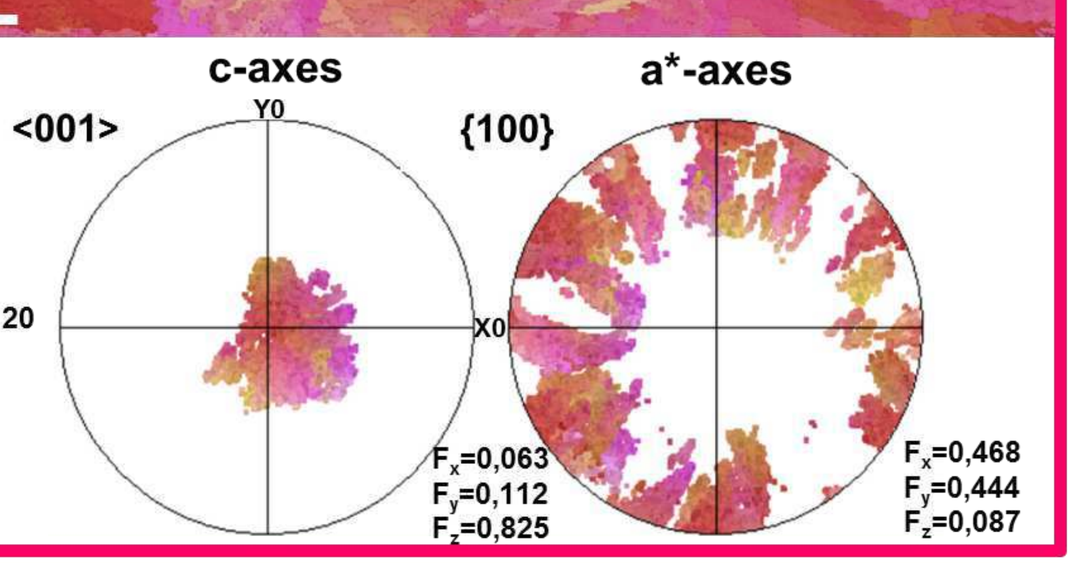
c-axes
a*-axes
<001>
Y0
{100}
X0
Fx=0,063
Fy=0,112
Fz=0,825
Fx=0,468
Fy=0,444
Fz=0,087

C


A

B

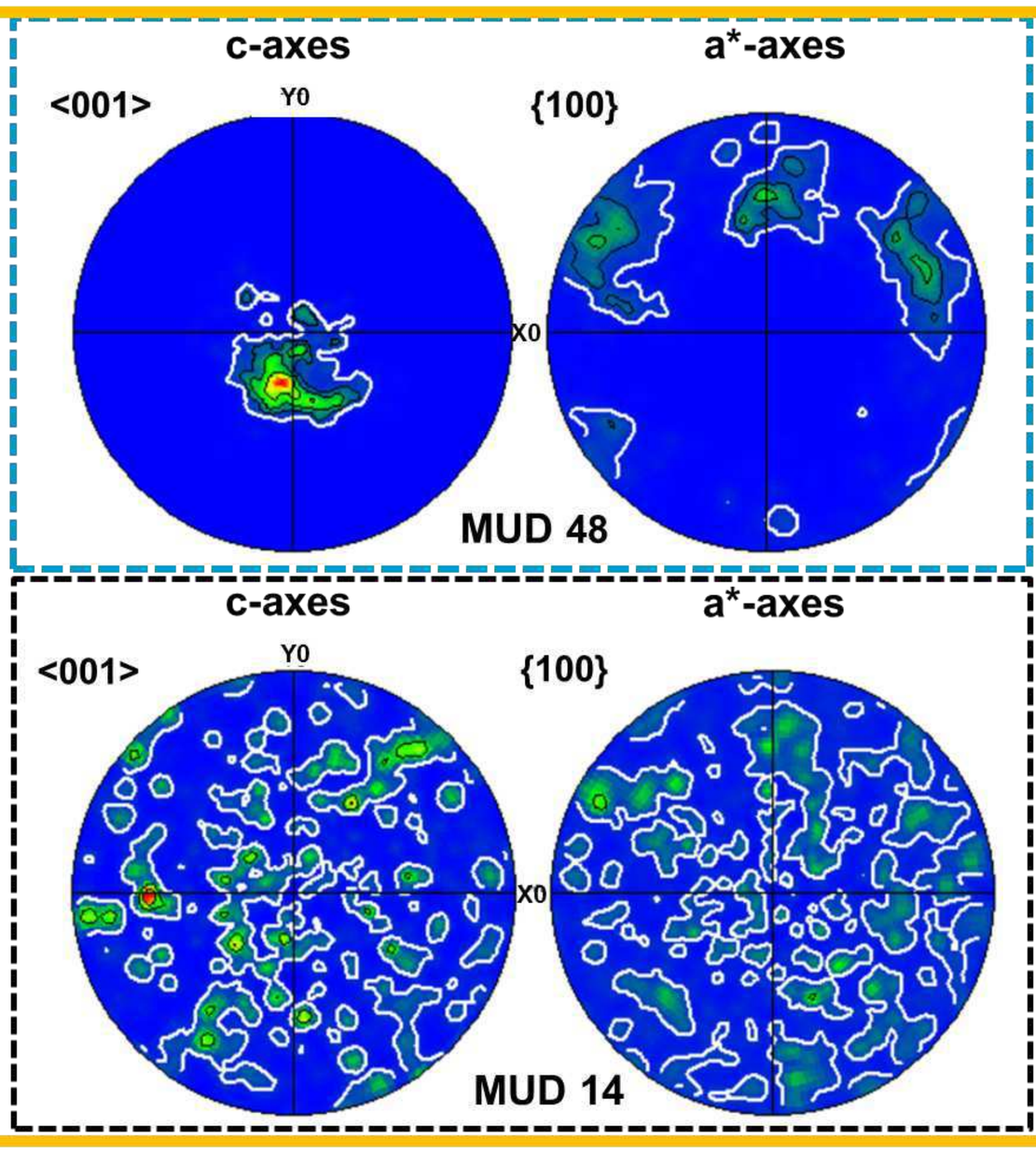
c-axes
a*-axes
<001>
Y0
{100}
X0
MUD 48
c-axes
a*-axes
<001>
Y0
{100}
X0
MUD 14

C

D

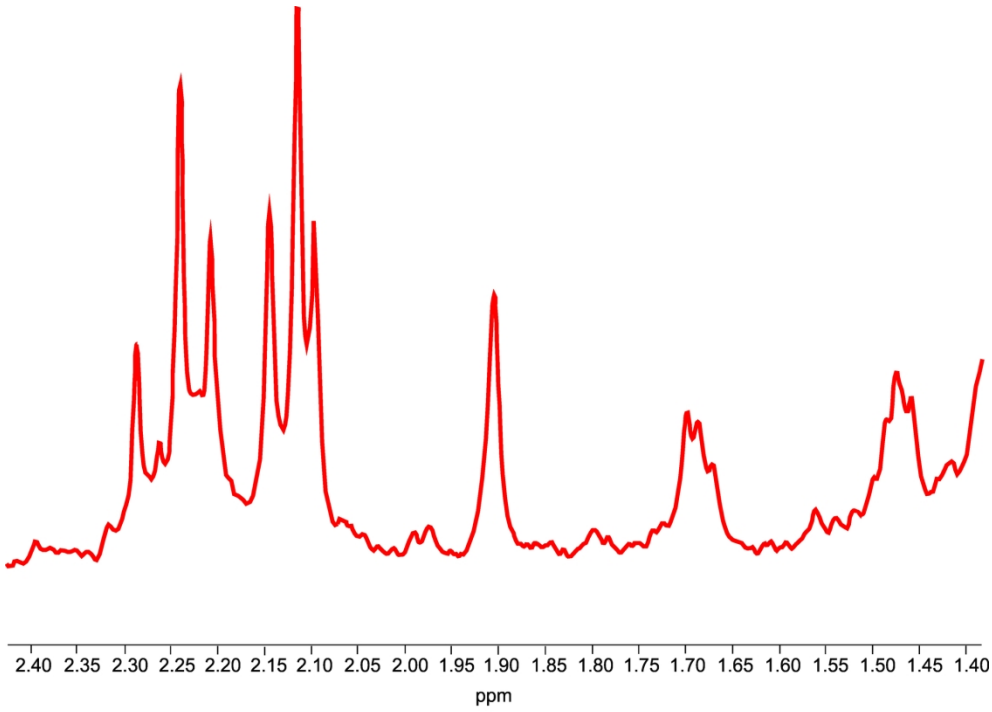

Figure 8

186x226mm (300 x 300 DPI)

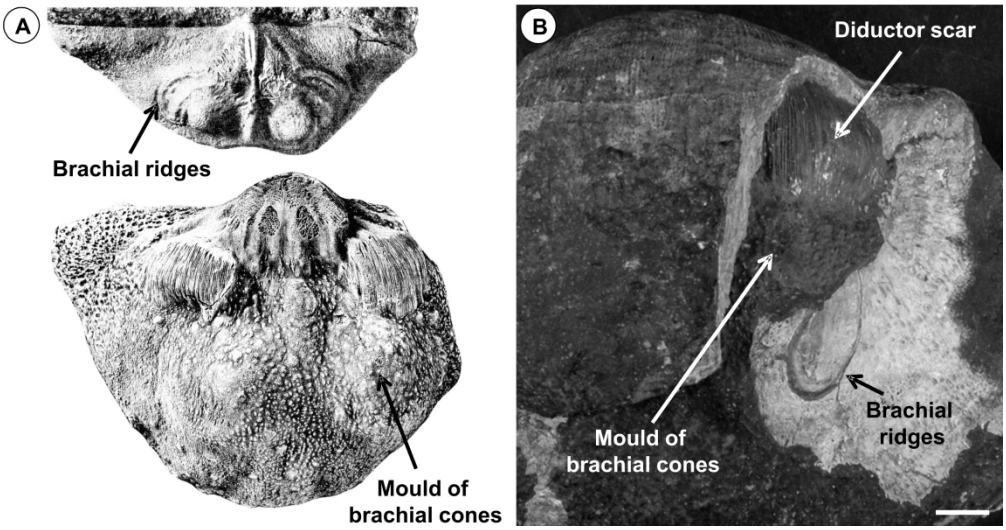
A
Brachial ridges
Mould of
brachial cones
B
Diductor scar
Mould of
brachial cones
Brachial
ridges

Figure 9

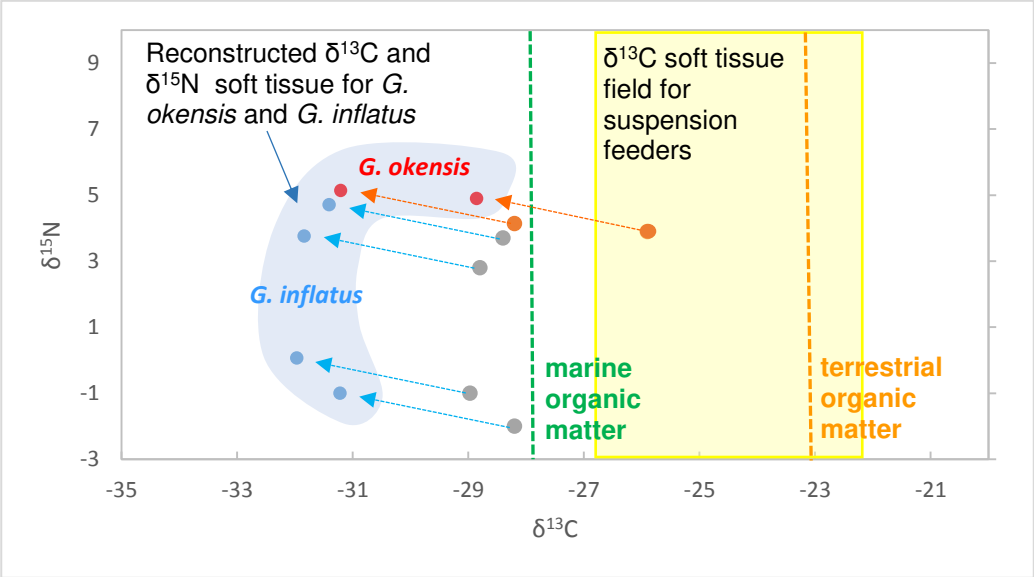
Reconstructed δ13C and δ15N soft tissue for G. okensis and G. inflatus
δ13C soft tissue field for suspension feeders
G. okensis
G. inflatus
marine organic matter
terrestrial organic matter
δ15N
δ13C
9
7
5
3
1
-1
-3
-35
-33
-31
-29
-27
-25
-23
-21

Species of *Gigantoproductus*					
Specimen	Taxon	Width (mm)	Length (mm)	Area	Log
RCK 5	*Gigantoproductus* sp.	153.2	59.1	9054.1	4
RCK 40	*G. okensis*	134.8	60.1	8101.4	3.9
RCK 25	*G. okensis*	120.2	59.3	7127.9	3.9
RCK 22	*Gigantoproductus* sp.	152.8	69.8	10665.4	4
RCK 9	*G. okensis*	120.2	65.2	7837.0	3.9
RCK 42 A	*G. okensis*	142.4	87.7	12488.5	4.1
RCK 16	*G. okensis*	122.8	88.3	10843.2	4
RCK 36 B	*G. okensis*	188.2	72.1	13569.2	4.1
RCK 13	*G. okensis*	145.2	81.8	11877.4	4.1
RCK 15	*G. okensis*	122.8	94.6	11616.9	4.1
RCK 203	*G. inflatus*	171.8	87.1	14963.8	4.2
OAW 224	*G. elongatus*	120.2	86.9	10445.4	4
OAW 236	*G. elongatus*	116.4	84.3	9812.5	4
OAW 207	*G. elongatus*	102.2	68.4	6990.5	3.8
OAW 218	*Gigantoproductus* sp.	138.2	81.7	11290.9	4.1
OAW 202	*G. elongatus*	118.2	71.2	8415.8	3.9
OAW 229	*Gigantoproductus* sp.	112.6	74.1	8343.7	3.9
OAW 227	*G. elongatus*	147	103.8	15258.6	4.2
RCK 225	*G. elongatus*	244.6	77.3	18907.6	4.3
OAW 7	*G. elongatus*	126.2	71.2	8985.4	4
OAW 25	*G. elongatus*	119.8	75.1	8997	4
OAW 21	*G. inflatus*	145.2	86.1	12501.7	4.1
OAW 12	*G. elongatus*	152.2	79.3	12069.5	4.1
OAW 10	*Gigantoproductus* sp.	168.6	100.1	16876.9	4.2
OAW 17	*Gigantoproductus* sp.	148.2	97.3	14419.9	4.2
RCK 228	*G. okensis*	94.4	74.2	7004.5	3.8
IBL 122	*G. okensis*	123.6	94.4	11667.8	4.1
IBL 123	*Gigantoproductus* sp.	93.2	68.4	6374.9	3.8
RCK 200	*G. inflatus*	163.2	126.2	20595.8	4.3
RCK 201	*G. inflatus*	133.2	78.6	10469.5	4
OAW 242	*G. okensis*	131.6	63.4	8343.4	3.9
OAW 241	*G. elongatus*	179.8	68.4	12298.3	4.1
OAW 226	*G. okensis*	116.4	100.6	11709.8	4.1
IBL 120	*G. okensis*	74.4	62.4	4642.6	3.7
OAW 216	*G. okensis*	118.2	67.5	7978.5	3.9
OAW 27	*G. elongatus*	152.4	89.4	13624.6	4.1
OAW 104	*G. inflatus*	112.4	87.4	9823.8	4
OAW 500	*Gigantoproductus* sp.	114.4	82.6	9449.4	4
OAW 2	*G. elongatus*	110.4	70.4	7772.2	3.9
OAW 3	*G. inflatus*	132.4	85.7	11346.7	4.1
OAW 8	*G. inflatus*	173.2	124.4	21546.1	4.3
OAW 50	*G. inflatus*	121.4	96.9	11763.7	4.1
OAW 6	*G. inflatus*	94.8	62.6	5934.5	3.8
OAW 5	*G. inflatus*	129.6	93.5	12117.6	4.1
OAW501	*G. elongatus*	132.5	102.5	13581	4.1
OAW502	*G. elongatus*	131.1	80.7	10580	4
WI1	*Gigantoproductus* sp.	167.6	122.6	20547.8	4.3

RCK 9.A	*G. okensis*	115.2	78.6	9054.7	4
WI 3	*G. inflatus*	184.4	102.6	18919.4	4.3
WI 2A	*Gigantoproductus* sp.	146.4	75.4	11038.6	4
				total	201.7
Average log-transformed shell area 201.7/50 = 4					

Species of genera other than *Gigantoproductus*					
Specimen	Taxon	Width (mm)	Length (mm)	Area	Log
RCK 42 C	*Latibrachythyris*	36.8	19.3	710.2	2.9
IBL 108	*Antiquatonia*	37.6	16.8	631.7	2.8
RCK 217	Linoproductinae	39.6	17.1	677.2	2.8
RCK 218	*Latibrachythyris*	24.8	23.2	575.4	2.8
OAW 210	Linoproductinae	30.4	15.4	468.2	2.7
OAW 243	*Latibrachythyris*	31.6	17.1	540.4	2.7
OAW 247	Tolmatchoffiini	18.8	11.4	214.3	2.3
RCK 211	*Antiquatonia*	43.6	23.2	1011.5	3
RCK 17 -1	*Girtyella*	6.6	9.9	65.3	1.8
RCK 17 - 2	Tolmatchoffiini	10.8	14.8	159.8	2.2
RCK 15 -1	*Latibrachythyris*	9.2	10.6	97.5	2
RCK 15 - 2	*Girtyella*	9.4	12.1	113.7	2.1
RCK 15 -4	*Antiquatonia*	25.6	15.6	399.4	2.6
RCK 15 - 5	*Latibrachythyris*	4.6	5.2	23.9	1.4
RCK 15 -6	*Harttella*	8.2	8.6	70.5	1.8
RCK 15 -7	*Antiquatonia*	14.8	22.2	328.6	2.5
RCK 15 - 8	Girtyellinae	5.6	7.2	40.3	1.6
RCK 15 -9	*Phricodothyris*	12.2	6.8	83	1.9
RCK15-10	*Krotovia*	19.2	15.8	303.4	2.5
RCK 15 -11	*Antiquatonia*	24.8	15.7	389.4	2.6
RCK 15 -12	Tolmatchoffiini	11.6	17.2	199.5	2.3
RCK 15 -14	*Harttella*	9.6	8.4	80.6	1.9
RCK 15 -18	*Girtyella*	9.2	12.4	114.1	2.1
RCK 15 -19	*Pleuropugnoides*	10.8	11.4	123.1	2.1
RCK 15 -26	*Girtyella*	6.4	7.6	48.6	1.7
RCK 15-27	Girtyellinae	6.2	6.8	42.2	1.6
RCK 15 -29	*Pleuropugnoides*	19.8	11.4	225.7	2.4
RCK 15 -33	*Phricodothyris*	8.6	7.4	63.6	1.8
WI -1	Girtyellinae	23.8	21.4	509.3	2.7
WI -2	*Antiquatonia*	42.4	39.2	1662.1	3.2
WI -3	Girtyellinae	6.1	5.1	31.1	1.5
WI -4	*Echinoconchus*	48.4	23.6	1142.2	3.1
WI -6	*Latibrachythyris*	34.2	27.4	937.1	3
WI -8	*Antiquatonia*	41.2	34.9	1437.9	3.2
WI-10	*Phricodothyris*	21.1	16.8	354.5	2.5
WI -14	*Antiquatonia*	42.8	34.9	1493.7	3.2
WI -15	*Echinoconchus*	46.8	24.8	1160.6	3.1
WI -16	*Pleuropugnoides*	21.4	18.4	393.8	2.6
WI -17	*Antiquatonia*	45.2	35.4	1600.1	3.2
3OCM -OAW	*Phricodothyris*	24.8	20.4	505.9	2.7
WI 1-1	*Echinoconchus*	52.4	38.8	2033.1	3.3

WI 1-2	*Antiquatonia*	46.4	28.1	1303.8	3.1
WI 1-3	*Antiquatonia*	45.2	29.2	1319.8	3.1
WI 1-4	Girtyellinae	9.8	12.4	121.5	2.1
WI 1-5	*Antiquatonia*	21.2	11.4	241.7	2.4
WI 1-6	*Antiquatonia*	12.6	11.8	148.7	2.2
WI 1-7	*Echinoconchus*	46.6	49.4	2302	3.4
WI 1 -8	*Echinoconchus*	53	48.2	2554.6	3.4
WI 1 -9	*Antiquatonia*	21.6	13.6	293.8	2.5
WI 1 -10	*Latibrachythyris*	23.8	20.2	480.8	2.7
WI 1 -11	*Latibrachythyris*	21.6	16.4	354.2	2.5
WI 1-12	*Phricodothyris*	20.8	15.6	324.5	2.5
WI 1-13	*Latibrachythyris*	34.4	23.8	818.7	2.9
WI 1- 14	*Antiquatonia*	48.4	31.8	1539.1	3.2
WI 1- 15	*Antiquatonia*	10.2	13.2	134.6	2.1
WI 1-22	*Echinoconchus*	45.8	35.1	1607.6	3.2
WI 1 -25	*Antiquatonia*	38.3	26.9	1030.3	3.0
WI 1 -28	*Echinoconchus*	48.2	46.5	2229.2	3.3
WI 1-33	*Pleuropugnoides*	20.5	17.5	358.7	2.5
WI 1 - 36	*Latibrachythyris*	28.2	18.7	537.3	2.7
WI 2-1	*Latibrachythyris*	42.4	28.3	1199.9	3.1
WI 2- 2	*Antiquatonia*	43.6	28.2	1229.5	3.1
WI 2 -3	*Antiquatonia*	38.4	29.2	1121.3	3
WI 2 -4	*Latibrachythyris*	43.2	25.8	1114.6	3
WI 2- 5	*Antiquatonia*	35.6	23.6	840.2	2.9
WI 2 -6	Girtyellinae	5.1	3.8	19.4	1.3
WI 2 -7	*Echinoconchus*	21.4	17.6	376.6	2.6
WI 2 -8	*Echinoconchus*	46.8	46.6	2180.9	3.3
WI 3 - 2	Girtyellinae	3.96	2.34	92664	1
WI 4 - 6	Girtyellinae	2.76	2.42	66792	0.8
					165.5
Average log-transformed shell area 165.5/69= 2.4					

Table 2 (NL Non luminescent; BL Bright luminescent; WL Weak luminescent; DL Dull Luminescent)

Sample #	Species Name	SEM analysis	Cathodoluminescence analyses	Weight (g)	$\delta^{13}C$ (‰ VPDB)	$\delta^{18}O$ (‰ VPDB)
OAW3	*G. inflatus*	preserved laminar layer; well preserved columnar layer; localized silicification at the outer margin of the columnar layer	NL, except BL at the outer margin of the columnar layer where silicification occurs (1 mm wide belt parallel to margin), along some growth lines close to the outer and inner margins and in microfractures (a few µm wide) parallel to intercrystalline boundaries	1.3	+0.8	-4.6
OAW203	*G. elongatus*	well preserved columnar layer; limited silicification at the outer margin of the columnar layer	NL, except BL at the outer margin of the columnar layer where silicified; along some growth lines and intercrystalline boundaries close to the outer margin	1.5	+1.1	-4.3
OAW212	*G. inflatus*	preserved laminar layer; well preserved columnar layer; localized silicification at the outer margin of the columnar layer	NL, except localized BL along growth lines and intercrystalline boundaries	1.4	+0.6	-4.7
RCK16	*G. okensis*	poorly preserved laminar layer; well preserved columnar layer; localized silicification at the outer margin	NL, except localized BL along growth lines	1.2	+2.3	-4.1
RCK33	*G. inflatus*	preserved laminar layer; well preserved columnar layer; localized silicification at the boundary between columnar and laminar layer	NL, except BL at laminar layer and boundary with columnar layer where silicification occurs; along some growth lines close to inner and outer margins, at intercrystalline boundaries and fractures crossing the valve perpendicularly	1.7	+2.0	-4.3
RCK35	*G. inflatus*	poorly preserved laminar layer; well preserved columnar layer; localized silicification at the outer and inner margin of the columnar layer and at the boundary with the laminar layer where present	NL in the intermediate portion of ventral valve; BL at inner and outer margin of columnar and laminar layers, along growth lines. One fracture crossing the valve with DL sparite followed by euhedral rhombic dolomite with a NL nucleus followed by BL growth phase	2.1	+1.6	-4.7
RCK36	*G. okensis*	preserved laminar layer; well preserved columnar layer; localized	NL, except BL at laminar layer, outer margin of columnar layer where silicified, along marginal growth lines and in a microfracture (µm wide)	1.3	+1.7	-3.9

		silicification at the outer margin	crossing the valve parallel to intercrystalline boundaries of the columnar layer			
RCK41	*G. inflatus*	no laminar layer; well preserved columnar layer; localized silicification at the outer margin	Largely N, except at the outer margin of columnar layer where silicified (0.5-1 mm wide zone parallel to margin); WL along 4 growth lines towards the inner margin and in the central part of columnar layer; fractures crossing the ventral valve perpendicularly, filled by BL sparite	0.5	+2.4	-3.5
RCK221	*G. inflatus*	well preserved columnar layer; localized silicification at the outer and inner shell margin	NL, except WL at growth lines close to the margins	2.6	+1.9	-3.8
RCK300	*G. inflatus*	poorly preserved laminar layer; well preserved columnar layer; localized silicification at the outer margin	NL, except BL along growth lines and intercrystalline boundaries	2.2	+2.6	-3.4

OurLabID	Sample ID	Species	$\delta^{15}N_{air}$ of Peak	%N of Sample Analysis	$\delta^{13}C_{VPDB}$ of Peak	%C of Sample Analysis
G-14044	1 - RCK16	*G. okensis*	+3.9	0.6	-28.2	71.6
G-14044	1 - RCK16	*G. okensis*	+4.4	0.7		
G-14046	3 - RCK33	*G. inflatus*	-1.8	2.9	-28.2	65.3
G-14046	3 - RCK33	*G. inflatus*	-2.2	2.9		
G-14047	4 - RCK36	*G. okensis*	+3.9	1.3	-25.9	70.2
G-14048	5 - RCK41	*G. inflatus*	+3.7	1	-28.4	83.3
G-14049	6 - RCK300	*G. inflatus*	+2.7	0.7	-28.8	80.1
G-14049	6 - RCK300	*G. inflatus*	+2.8	0.8		
G-14052	9 - OAW212	*G. inflatus*	-0.9	2.4	-29	66.6